## Author's Response to referee #1:

We wish to thank referee #1 for the comprehensive and constructive comments providing the opportunity to improve our manuscript. The comments led to a major revision of the manuscript. For convenience, our response is given by order of appearance following the structure of the manuscript.

## 1.Introduction

Referee's comment:
P2, L46: The mentioned advantage of ceilometers over lidars must be specified! Regarding what? .... is the question! If I would have to select, I would take a sophisticated lidar because such a system is much more powerful concerning emitted pulse energies and the list of aerosol products is long compared to quite 'simple' and 'weak' ceilometers. So, please specify what you definitely mean, ... with advantage! Probably low costs, robust observations, no complex adjustments, and calibrations. However, the clear disadvantage of ceilometers, operated at water vapour absorption around 910 nm, is that the only product you can trust is the range-corrected signal, nothing else!
Author's response:
Comment accepted.
Author's changes in manuscript:
Additional text in Sect.1 (Introduction):
" Applicable evaluation of PBL heights can be derived either by actual measurements or estimations based on numerical weather prediction (NWP) models. On the one hand, NWP models, such as regional models, provide high temporal and spatial data resolution beyond the capability of actual measurements. On the other, they are based on mathematical equations with initial assumptions and boundary conditioned set beforehand. Hence, the models' products require a systematic validation tool based on actual measurements.

There are two main PBL height measurement methods: in-situ radiosonde launches and remote sensing such as lidars and profilers. Unfortunately, radiosonde launches are costly as successive measurements. Profilers and sophisticated lidars produce high temporal resolution profiles but are limited in space. Moreover, certain meteorological conditions may reduce their performance, such as precipitation for radio acoustic sounding system profilers (Uzan et al., 2012) and dust storms for Raman lidars (Mamouri et al., 2016).

These limitations have led several research groups to successfully utilized ceilometers - single wavelength cloud base height detectors, as a means to recognize and determine the PBL height (Eresmaa et al., 2006, Haeffelin and Angelini, 2012, Wiegner et al., 2014). Ubiquitous in airports and meteorological service centers worldwide, ceilometers obtain a wide spatial resolution per lidar (for further information see TOPROF of COST Action ES1303 and E-PROFILE of the EUMETNET Profiling Program). They produce high temporal resolution profiles about every 15 s and every 10 m, up to several km, retrieved as attenuated backscatter signals. The ceilometers are low cost, easy to maintain, and operate continuously unattended under diverse meteorological conditions (Kotthaus and Grimmond, 2018). These qualities reflect their advantages over high-cost, multi-wavelength sophisticated lidars, that require

surveillance, calibration procedures, and careful maintenance. Hence, they are limited in space and operational time (Mamouri et al., 2016) and cannot achieve the spatial and temporal measurements coverage essential to validate the PBL heights generated by NWP models.".

## 2.Research area

Referee's comment:

P4, L92: Please provide longitude, latitude and height above sea level for Beit Dagan already here, and where is it located (including distance) with respect to Tel Aviv and Jerusalem.

Author's response:

The location and topography of Beit Dagan were given in Fig. 1 and Table 1. Following the referee's remark, the radiosonde parameters were added to the text given in Sect. 4.2.

Author's changes in manuscript:

(1) Text in Sect. 4.2 (Radiosonde): "The Israeli Meteorological Service (IMS) obtains systematic radiosonde atmospheric observations twice daily, at 23 UTC and 11 UTC, adjacent to a ceilometer. Launching is performed in Beit Dagan (32.0 ° long, 34.8 ° lat, 33 m a.s.l), situated 7.5 km east from the shoreline, 11 km southeast to Tel Aviv, 45 km northwest to Jerusalem (Fig.1 and Table 1)".

(2) Changes in Table 1:
   a. Title: "Location of measurement sites and ceilometer types".
   b. Affiliation: Beit Dagan $(BD)_b$- [b]The location of ceilometer Beit Dagan and the radiosonde launch site.

(3) Changes in the caption of Fig. 1:" … The Radiosonde launch site is situated in Beit Dagan, adjacent to the ceilometer ".

Referee's comment:

P4, L109: Please provide frequently, what UTC means in local time. Local time is needed to better follow the discussion on PBL evolution and the diurnal cycle.

Author's response:

Comment accepted.

Author's changes in manuscript:

UTC was corrected to LST winter time (corresponding to UTC+2) in the paragraph describing the Israeli summer PBL evolution (Sect.2 Research area).

Referee's comment:

P4, L110-120: There is no general PBL diurnal cycle in Israel, I speculate. But you provide such an impression! The occurrence, onset, strength, and impact of the sea breeze circulation depend on given meteorological conditions (marine westerly versus continental easterly air flows, low and high wind speeds, clear or cloudy conditions). The sea breeze event strongly influences the PBL diurnal cycle. All this must be carefully mentioned in the text. And what about the impact of dense desert dust layers (in the PBL and especially in the free troposphere)? Is there any PBL development when there is a dust outbreak event? So all in all, many factors

seem to control the sea breeze events and the PBL cycle in Israel. Thus, please provide more details on this.

Author's response:

The description of the PBL diurnal cycle refers solely to the Israeli summer as stated in the text (line 105): "Comprehensive research of the Israeli summer PBL…".

In the summer, the east Mediterranean is dominated by rather persistent synoptic systems explained in lines 104-107: " … a persistent Persian Trough (either deep, shallow or medium) followed by a Subtropical High aloft (Alpert et al., 2004)", combined with the sea breeze circulation. These conditions generate the PBL height diurnal cycle described in the manuscript and presented in Fig. 1 and Fig.2 from Levy et. al., (2011) and Uzan et. al., (2012), respectively. In these figures, the diurnal PBL was obtained by signal to noise measurements and virtual temperature profiles from an acoustic radar. The radar was stationed in flat terrain, 3.5 km inland from the shoreline, 51 km north to Beit Dagan. In Uzan et al, (2012) the profiles were classified by the three dominant summer synoptic systems at the time of research (Jun-Oct, 1997-1999, 2002-2005). Levi et al produced the average diurnal evolution for the month of July between 1997-1999".

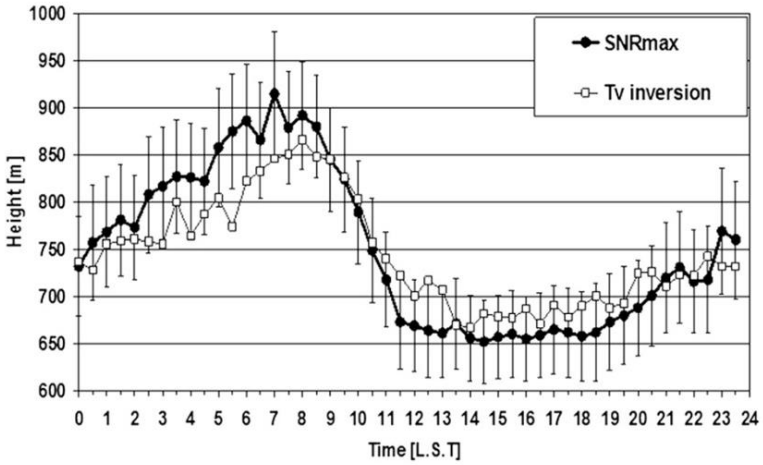


Fig.1 The average diurnal evolution of the boundary layer height during Julys of 1997–99 as defined by the height of SNRmax value (filled circles) together with the upper and lower 95% confidence limits. The inversion in the corrected virtual temperature $T_v$ measured by the RASS is indicated by open squares.

(Source: Levi et al., 2011)

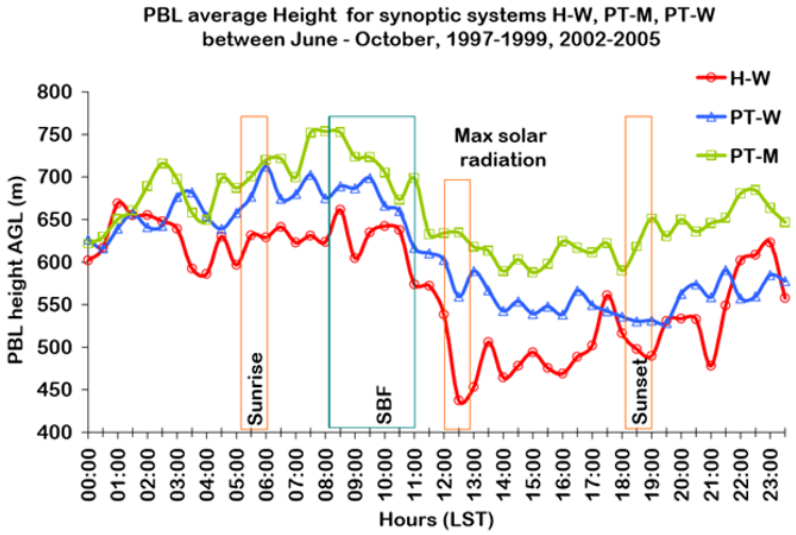


Fig.2 Lap-3000 profiler results of the average PBL height for the three main synoptic systems, Persian trough weak (PT-W, blue line, an average of 347 days), Persian trough medium (PT-M, green line, an average of 232 days) and High to the west (H-W, red line, an average of 198 days), during June-October 1997-1999,2002-2005. Also indicated are times of sunrise and sunset, maximum solar radiation and SBF entrance. (Source: Uzan et al., 2012)

Concerning dust outbreak events, Alpert et al. (2002) investigated dust forcing over the eastern Mediterranean. They concluded: "Summer outbreaks of dust over the Eastern Mediterranean are relatively rare. This area gets frequent intrusions of dust in spring (Alpert and Ziv 1989; Alpert et al. 2000; Moulin et al. 1997) with a secondary maximum in the autumn (Ganor 1994). The dynamical system that transports the dust is primarily the Sharav cyclone, which is also called the Saharan depression, generated in the lee of the Atlas Mountains (Egger et al. 1995) and moving along the North African coast eastward (Alpert et al. 1990b). The Sharav cyclone is clearly not the associated synoptic system in summer". Moreover, dust layers that were evident over Israel in the summer were located in high altitudes.

Author's changes in manuscript:

(1) Following the referee's remark, we rephrased the text to emphasize the description of the PBL diurnal cycle refers only to the Israeli summer season: " Previous research describes the formation and evolution of the Israeli summer PBL height as a function of the synoptic and mesoscale conditions, as well as the distance from the shoreline, and the topography. Overall, the diurnal PBL height in the summer season may be portrayed in the following manner.."

(2) Details about the occurrence of dust events in the summer were added to the text: " The Israeli summer season (June-September) is characterized by dry weather (no precipitation), high relative humidity (RH) - up to 80% in midday in the shoreline (Israeli Meteorological Service -IMS weather reports) and sporadic shallow cumulus clouds. On the synoptic scale, the summer is defined by a persistent Persian Trough (either deep, shallow or medium) followed by a Subtropical High aloft (Felix Y., 1994,

Dayan et al., 2002, Alpert et al., 2004). Combined with the sea breeze, the average PBL height is found to be quite low. For example, the average summer PBL height in Beit Dagan (33 m a.s.l and 7.5 km east from the shoreline) reaches ~900 m a.g.l after sunrise, and before the entrance of the sea breeze front (Felix Y.,1994, Dayan and Rodinzki, 1999, Uzan et al., 2016, Yuval et al., 2019). Summer dust outbreaks in the eastern Mediterranean are quite rare (Alpert and Ziv 1989, Alpert et al., 2000) therefore, they were not addressed here, especially in the height levels below 1 km (Alpert et al., 2002)".

**(3.IFS and COSMO Models- no comments)**

**4.Instruments**

Referee's comment:

P6, L161: Why should single-wavelength lidars not allow the retrieval of mass concentration profiles ... from proper profiles of particle optical properties? Sure, they can be used for this. Ok, this is not the topic of the paper. But the statement is wrong and should be removed. The ceilometer on the other hand side cannot be used to derive proper optical and microphysical properties. That is true! A ceilometer can only be used to detect aerosol layers as a function of height. This is not much, but sufficient for PBL studies. That should be clearly mentioned.

Author's response:

In order to differentiate and define the composition of atmospheric aerosols, various wavelengths corresponding to different characteristics are necessary. Weigner et al., (2014) further explains: "Whereas the detection of aerosol layers and their vertical extent requires only simple single-wavelength backscatter lidars, the derivation of extinction coefficient profiles and a series of intensive aerosol properties requires advanced lidar concepts such as high-spectral resolution lidars (HSRL, Shipley et al., 1983) or Raman lidars (Ansmann et al., 1992)". Nonetheless, Weigner succeeded to produce satisfactory estimations of the attenuated coefficient based on signal calibrations and corrections for water vapor absorption (Weigner and Gasteiger, 2015).

Author's changes in manuscript:

" One drawback is that calibration procedures were nonexistent in all sites, and in most cases, maintenance procedures (cleaning of the ceilometer window) were not regularly carried out, with the exception of the IMS Beit Dagan ceilometer. Nevertheless, the PBL height detection is based on a pronounced change of the attenuated backscatter profile. This change is attributed to variations in the aerosol content providing indications for both clouds and atmospheric layers. Therefore, the limitation of a single wavelength within the spectral range of water vapor absorption does not affect this type of detection. In order to derive the backscatter coefficient from ceilometer measurements, signal calibrations and water vapor corrections are necessary (Weigner et al., 2014, Wiegner and Gasteiger, 2015)".

Referee's comment:

P7, L185: Please state again where Beit Dagan is located.

P8, L184-187: It should be clearly emphasized that the radiosonde provides ONE value for the PBL height, no diurnal cycle, ... nothing! Only a snapshot of the PBL height, a few minutes after launch is provided by the sonde! In contrast, models can produce the diurnal cycle, and ceilometers can measure it. But all this is not shown and discussed!

Author's response:

(1) Lines 184-185 state:" Radiosonde (RS) type….is launched twice daily at 23 UTC and 11 UTC by the IMS in the Beit Dagan site, adjacent to the ceilometer".

(2) The time differences between the models and the ceilometers were mentioned in the text as follows:

   a) P 5, lines 146-147: "IFS profiles were limited to hourly resolution, while COSMO generated profiles every 15 minutes. To compare COSMO's PBL heights, a series of trials were performed to find the correct representation of hourly values as the last 15 minutes within an hour".

   b) P 6, lines 179-181: "To compare the hourly results of the models (Sect. 3), the ceilometers' 15 seconds profiles were averaged to half-hour ones, whereas the second half-hour profile within each hour was chosen".

Nonetheless, the relevant sections were rephrased to create a clearer explanation.

Author's changes in manuscript:

(1) Sect 4.2 (Radiosonde) was rephrased with additional information:
"The IMS obtains systematic radiosonde atmospheric observations twice daily, at 23 UTC and 11 UTC, adjacent to a ceilometer. Launching is performed in Beit Dagan (32.0 ° long, 34.8 ° lat, 33 m a.s.l), situated 7.5 km east from the shoreline, 11 km southeast to Tel Aviv, 45 km northwest to Jerusalem (Fig.1 and Table 1). The radiosonde, type Vaisala RS41-SG, produces profiles of RH, temperature, pressure, wind speed and wind direction as it ascends. Measurements are retrieved every 10 seconds, corresponding to about every 45 m, reaching 2 km in about 8 minutes. The horizontal displacement of the radiosonde depends on the intensity of the ambient wind speed. The average wind speed along the 11 UTC summer profiles is about 5 m/s (Uzan et al., 2012). Therefore, the horizontal displacement of the radiosonde from its launch position is fairly low and is estimated at about 2.5 km. Moreover, the radiosonde position resolution is defined as 0.01°. As aforementioned, the PBL height in Beit Dagan for midday summer is estimated below 1 km (Dayan and Rodinzki, 1999, Uzan et al., 2016, Yuval et al., 2019). Hence, within an ascending height of 1 km, the change in the radiosonde's horizontal position is under 0.01° which is an order of magnitude from the models' grid resolution. Thus, we assert the radiosonde profiles represent the Beit Dagan site and the displacement error of the ascending radiosonde can be neglected".

(2) A text was added to Sect. 6.1 (Comparison to in-situ radiosonde profiles):
"Statistical analysis of the Beit Dagan PBL heights mean error (ME), root mean square error (RMSE), and correlation (R) is presented in Fig. 2 and Table 3 for 11 UTC. The analysis was based on the comparison between radiosonde measurements at 11 UTC, to Beit Dagan ceilometer average profiles between 10:30-11:00 UTC, IFS estimations for 11 UTC and COSMO results for 10:45 UTC".

## 5.Methods

Referee's comment:
This chapter is much too long. Textbook knowledge is presented in unnecessary detail. For each method, please provide the equation, the explanation of the equation, the link to PBL height, and a proper reference. More is not needed. A short and compact section on methods is desirable.
Author's response:
Comment accepted.
Author's changes in manuscript:
The method section was edited in a concise manner.

Referee's comments:
P9, L247: This is confusing: A ceilometer is made to detect the base of the water cloud, but not to detect the cloud top height. In most cases of low level (liquid-water) clouds, there is no chance to detect the cloud top! This needs to be clearly stated. The maximum signal you measure cannot be interpreted as a cloud top. This is a very erroneous statement! The maximum backscatter signal is somewhere between the cloud base and cloud top. The maximum signal is at that height where the attenuation effect becomes so strong that the signal immediately drops to the sky background level. This needs to be clearly stated. The height of the maximum signal maybe 100, 300, or 1000 m below the cloud top. Nobody knows!
P10 L268: ...Therefore, also the following statement is wrong: Our algorithm denotes the PBL height as the top of the shallow cloud. As just mentioned, you are unable to see the cloud top with ceilometer, only exceptional, in cases with optically rather thin clouds. Please improve your statements. The discussion is unacceptable in the present form.
Author's response:
Thank you for this important remark.
In this research, we employed the wavelet covariance transform (WCT) method on the ceilometers' backscatter profiles. The principle of this method is to calculate the derivatives between measuring points along the length of the backscatter profile. The highest derivative implies a profound difference in the atmospheric aerosol content. On clear days, this difference occurs as the transmitted light exits the well-mixed layer and enters the stable layer above. In the presence of clouds, the highest values are retrieved at cloud base height which is considered as the mixed layer height. The cloud top denotes the bottom height of the free atmosphere (Fig.3 from Stull, 1988).

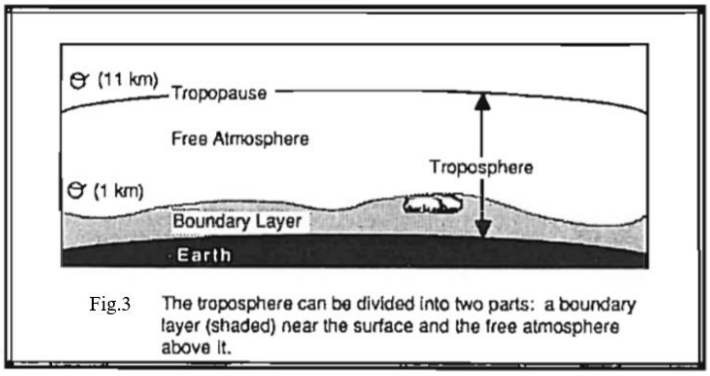


Fig.3 The troposphere can be divided into two parts: a boundary layer (shaded) near the surface and the free atmosphere above it.

(Source: Stull, 1988)

Therefore, in order to generate a consistent definition of the PBL height by the WCT method, our algorithm seeks the height of the transition zone in the presence of clouds as well. This height is defined here as the highest measuring point of a cloud above the cloud base height. Even though the summer clouds are relatively shallow (~ 500 m thickness based on observations, see example in Fig.4 and Fig.5), there is no guarantee the algorithm detects the actual cloud top. Therefore, to prevent misinterpretations, the phrase "cloud top" was omitted and clarified as the highest measurement point of a cloud above a cloud base height.


Fig.4 IMS photograph of the sky over Beit Dagan site on August 2, 2019, at 8 UTC presenting typical shallow cumulus clouds.

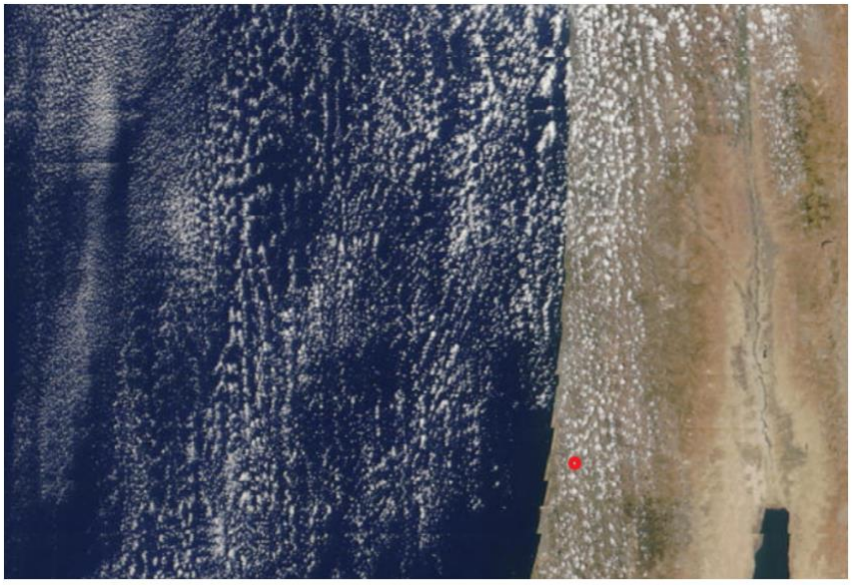

Fig.5 Terra-MODIS 250 m resolution picture over Israel on August 2, 2019, at 8 UTC. Beit Dagan site is indicated by a red dot. Adapted from @NOAA- EARTHDATA.

Author's changes in manuscript:
"When clouds are present (mainly summer shallow cumulous), the algorithm defines the highest measurement point of a cloud (above the cloud base height) as the height where the signal counts decrease to the amount retrieved by background values. This signifies the ceilometer's identification of the entrainment zone (Stull, 1988)".

## 6.Results

Referee's comment:
P10, L286, and Figure 3: This is the worst case you can select in a comparison paper. There is the PBL development, there is the sea breeze effect, and there is cloud evolution! As a consequence, the PBL depth is more or less undefined at these complex atmospheric conditions… This case study is rather confusing and not helpful. Unambiguous, cloud-free conditions would be desirable to check the different approaches of PBL height retrieval.
Author's response:
We analyzed a total of 33 cases and received good results for the majority of the data (cases of either cloud-free or sporadic shallow cumulus clouds). The largest gaps between the models' estimations and the radiosonde measurements were found on August 17, 2016, presenting an uncommon multi-layer summer cloud. As the referee correctly discerned, this complex meteorology explains the large gaps between the models and the instruments. We agree with the referee for the necessity to present a case reflecting the ability of the method. Therefore, we generated a new figure demonstrating a typical event to explain the method rather than the extraordinary results of Aug 17, 2016.
Author's changes in manuscript: Figures 3 and 5 were replaced by a typical event on August 15, 2015 (Fig. 6).

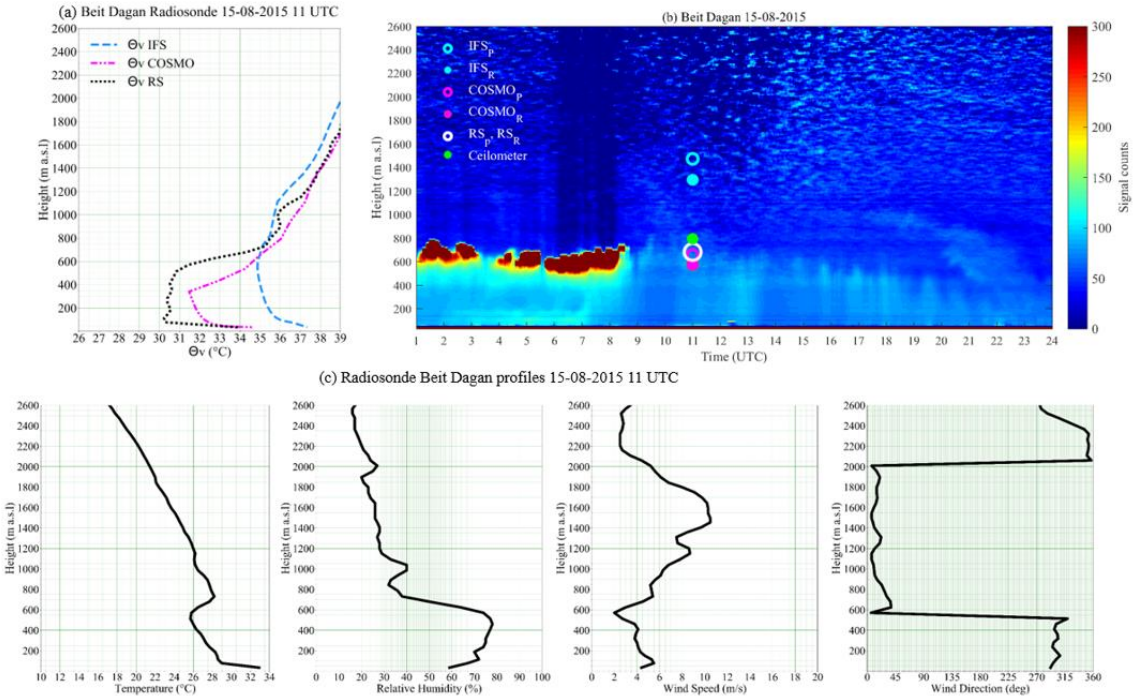


Fig.6 Meteorological measurements from Beit Dagan site on August 15, 2015: Virtual potential temperature profiles at 11 UTC generated from radiosonde measurements, IFS and COSMO models (a), ceilometer signal counts plot including indications of the PBL heights at 11 UTC from the models ($IFS_R$, $IFS_P$, $COSMO_R$, $COSMO_P$), radiosonde ($RS_R$, $RS_P$) and ceilometer (b). The bottom panel presents radiosonde profiles of temperature, RH, wind speed and wind direction at 11 UTC (c).

Referee's comment:

P10, L286, and Figure 3: Fortunately, the radiosonde temperature profile indicates the PBL height at about 800m because for this height range (from 50 – 800m) the layer is well mixed indicated by the almost height-independent virt. pot. temperature. Then the pot. Temperature strongly increases with height and prohibits vertical mixing higher up. However, in Fig.3, the PBL heights obtained by the authors (from radiosonde, ceilometer, COSMO and IFS model) are between 1000 and 2200m? This is confusing! The PBL height is clearly not at 1000m, 1400m, 1700m, or even 2000m. So, the ceilometer result of 1700m is totally wrong to my opinion. The reason is obviously that the range-corrected signal (and the wavelet analysis) cannot be used at these cloudy conditions to detect the true PBL height. What you see is some arbitrary height where the range-corrected signal takes its maximum...

Author's response:

The referee indicated the PBL height as the highest point aloft before the virt. pot. temperature increases. Following Stull (Fig.8 from Stull, 1988, Chapter 5, paragraph 5.5), and the parcel method (Holzworth 1964, Seidel et al., 2010) we indicated the PBL height as the height where the virtual potential temperature reaches the value that of the surface level. By this method, the PBL height is indicated as the height where the passage from the unstable layer to the stable layer above occurs. The unstable layer is defined by the mixed layer and the entrainment zone above. This definition corresponds with the height point at which an abrupt change is measured by the ceilometers, at the transition zone between the well-mixed layer and the free atmosphere above.

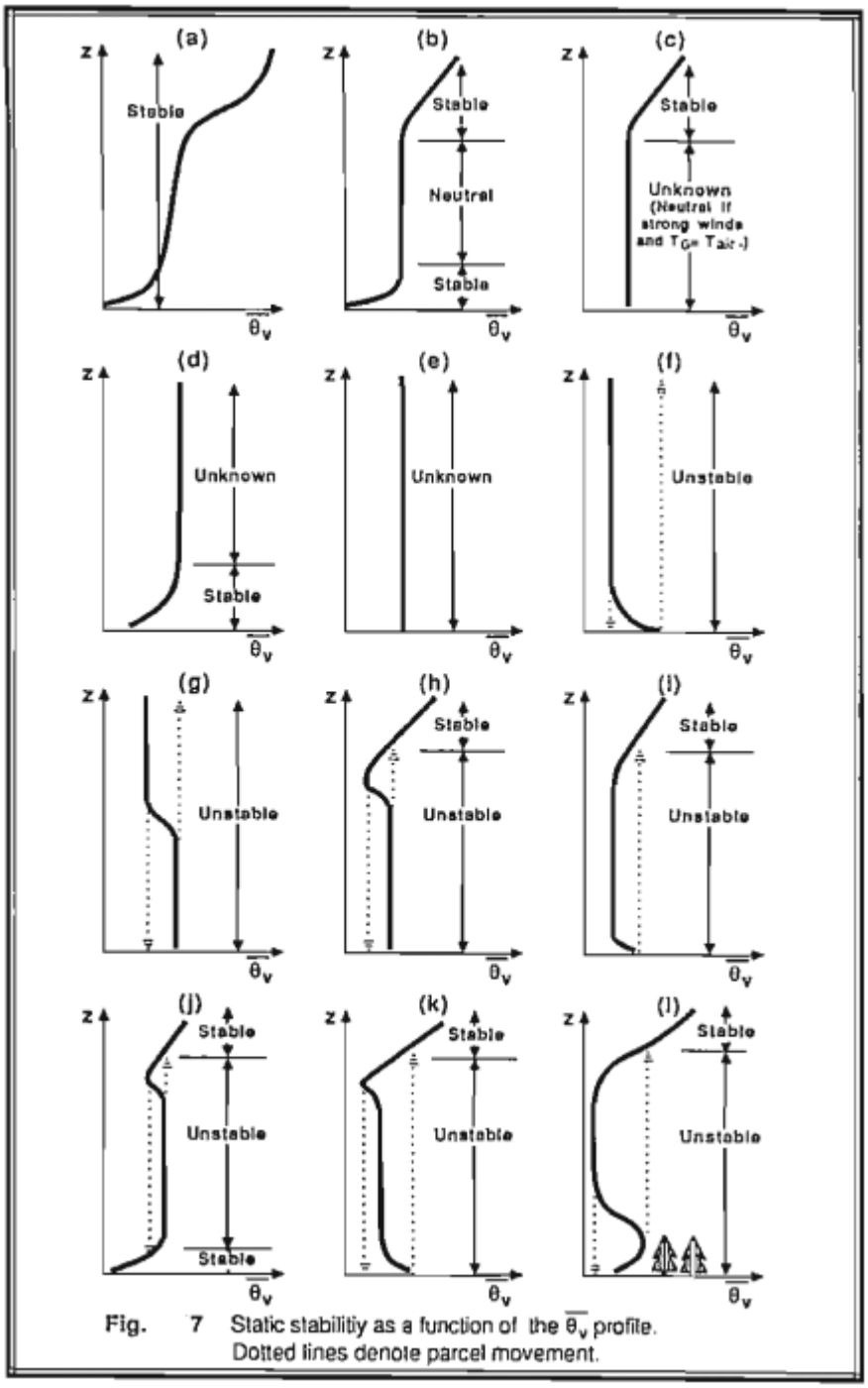


Fig. 7 Static stabilitiy as a function of the $\overline{\theta_v}$ profile. Dotted lines denote parcel movement.

We refereed to figure (k) and (I) corresponding to daytime summer static stability of the eastern Mediterranean.

Author's changes in manuscript:

No changes were made in the manuscript.

Referee's comment:

P10, L286, and Figure 3: If the radiosonde observations of temperature, relative humidity, wind speed, and wind direction would be shown, we would have the chance to see what is going on here. But all this is not presented. Height resolved trajectory analysis would be helpful as well in the discussion of the complex meteorological conditions. Please provide at least the wind and RH profiles of the radiosonde in the figures. The reader may want to know more about the meteorological situation.

Author's response:

Comment accepted. Profiles of temperature, RH wind speed and wind direction from the adjacent radiosonde launch site are given in Fig. 8 below.

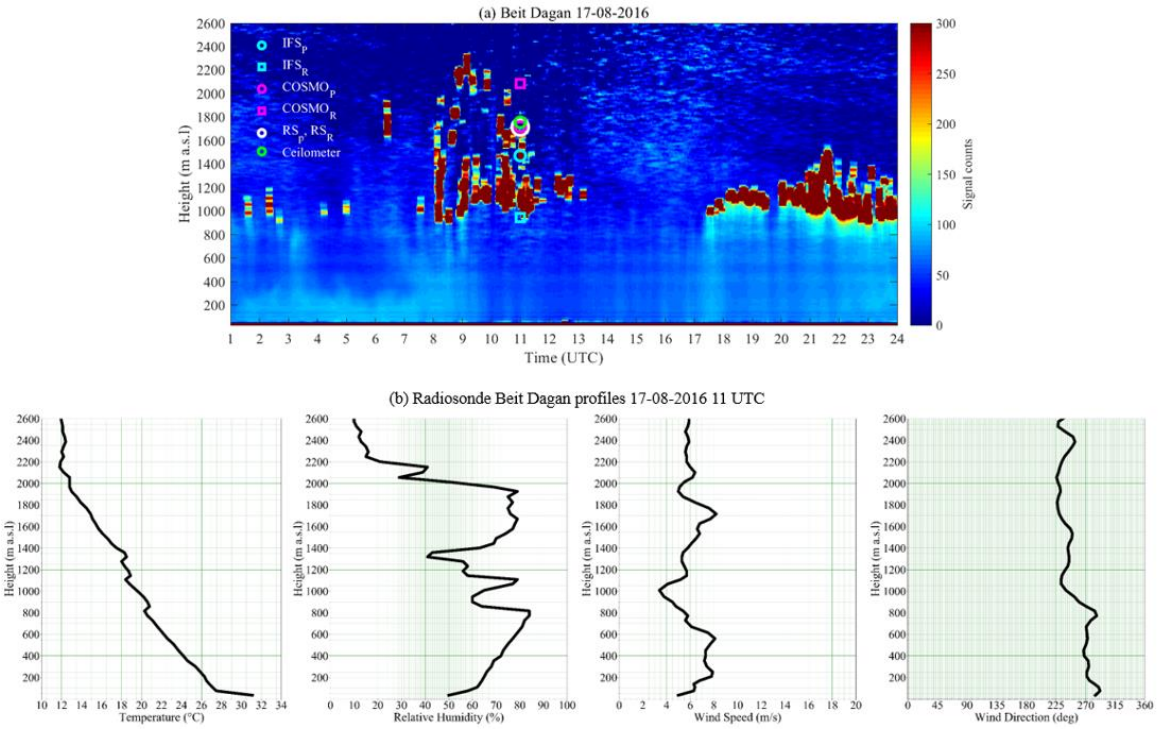


Fig.8 Ceilometer signal counts plot on August 17, 2016, including indications of the PBL heights at 11 UTC from the models ($IFS_R$, $IFS_P$, $COSMO_R$, $COSMO_P$), radiosonde ($RS_R$, $RS_P$) and ceilometer (a). The bottom panel presents the radiosonde profiles retrieved at 11 UTC on the same day (b).

Author's changes in manuscript:

Additional plots presenting radiosonde profiles of wind speed, wind direction, relative humidity, and temperature were added to the typical case on Aug 15, 2015.

Referee's comment:

P11, L308: Again, Figure 5 shows a rather difficult case (PBL evolution plus sea breeze effect). There is obviously a marine boundary layer (with the top at 600m, clearly seen by the radiosonde) and, on top, the upper part of continental PBL up to about 1500m (also visible in the radiosonde profile). But, per definition, the lower PBL counts (the lowest well-mixed layer above the surface is the boundary layer, as defined by Stull 1988). And that is the marine boundary layer, indicated by the potential temperature profile and the ceilometer data. But the PBL height obtained from the ceilometer profile analysis is again around 1700 m. This is an error of more than 100%! Please show RH and wind profiles (direction and speed) so that more information about the complex PBL development at sea breeze conditions is available. Again, the selected case and the discussion are rather confusing. The results are at all not convincing, and not understandable. What is then the message of the study? Obviously, the IFS model does not simulate the impact of the sea breeze impact correctly or even ignores sea breeze effects so that the continental pot. temperature profile is obtained with this model. The IFS PBL heights seem to be in contradiction with the IFS pot. temp. profile. The COSMO pot. temp. profile is in good agreement with the radiosonde profile and shows the PBL height at 600 m. Very stable conditions higher up are simulated with COSMO so that not vertical mixing is possible above 600 m height. Surprisingly, the COSMO PBL height is from 1700 to 2100 m. This is totally confusing! This seems to be simply a mistake! Please clarify!

Author's response:

We deeply apologize for this clerical error. The referee is correct. The figure contains a grave mistake. Unfortunately, the data of PBL heights of Aug 17, 2016, were mistakenly presented for Aug 10, 2015, as well. A correct figure including meteorological profiles from the adjacent radiosonde are given in Fig. 9 and Fig 10 below:

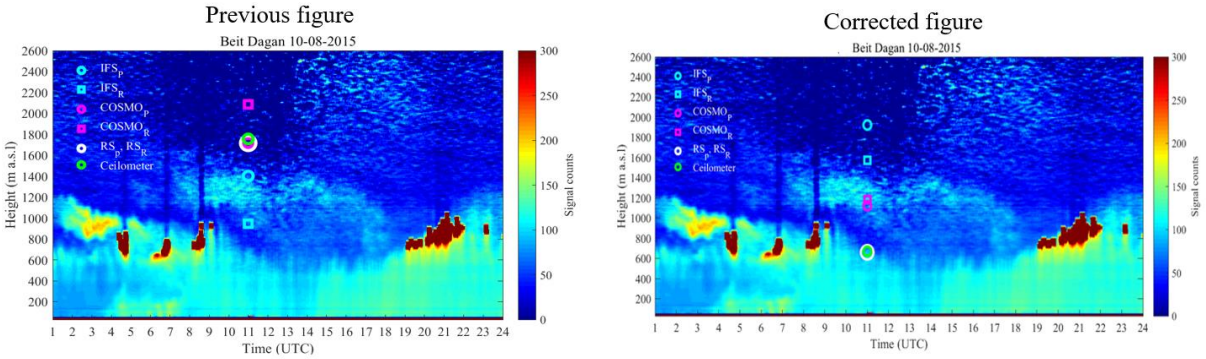


Fig.9 Before (left panel) and after (right panel) the correction of the figure describing Aug 10, 2015.

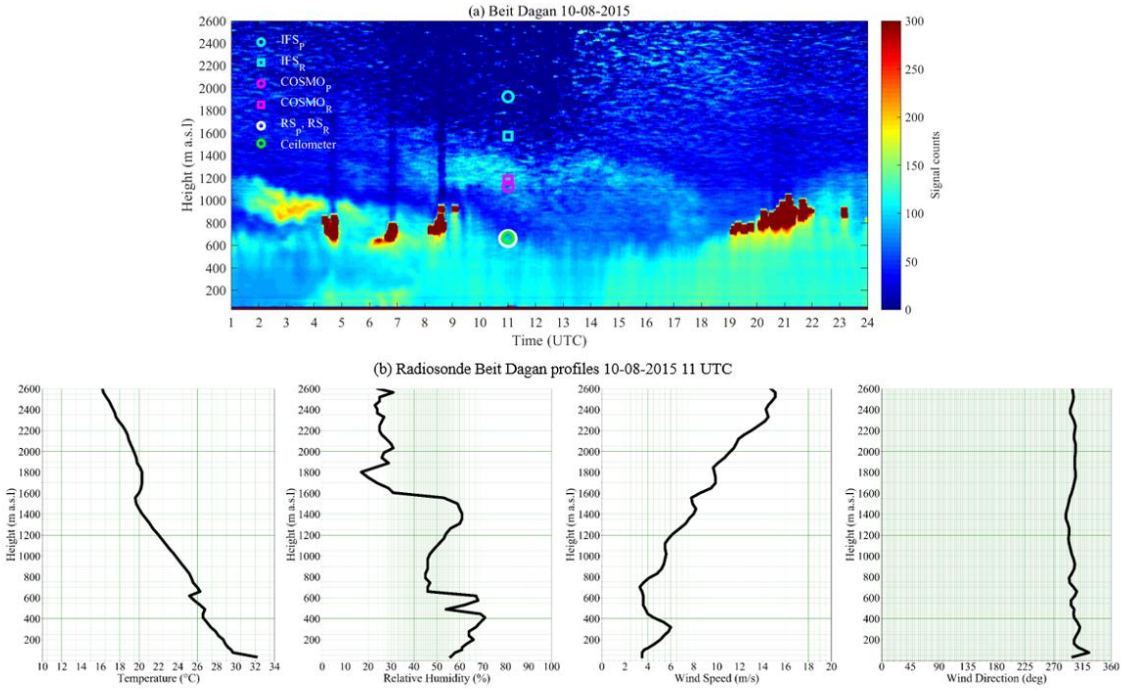


Fig.10 Ceilometer signal counts plot on August 10, 2015, including indications of the PBL heights at 11 UTC from the models ($IFS_R$, $IFS_P$, $COSMO_R$, $COSMO_P$), radiosonde ($RS_R$, $RS_P$) and ceilometer (a). The bottom panel presents the radiosonde profiles retrieved at 11 UTC on the same day (b).

Author's changes in manuscript:

The corrected figure including the meteorological conditions for each study case is given in the point to point response, but not in the manuscript. Following the referee's suggestion, they were replaced by a representative case of the method on August 15, 2015.

Referee's comment:

P12: Is section 6.3 needed? It is a very specific regression approach, just applicable to Israel.

Author's response:

Sect. 6.3 suggests a new approach to correct COSMO PBL height estimations by ceilometers. Actually, that is the goal of the research. The method proved as an applicable tool to validate and even correct the model's estimations. In regions with scarce profiling, there are no other alternatives to validate the model's results. Considering the simplicity of the method, it can be easily adapted in similar topographical areas by adjusting the correction factors (Eq. 6).

Author's changes in manuscript:

The paragraph was rephrased to emphasize the advantage and importance of the suggested method.

Referee's comment:

P12-13 The conclusions must be rewritten after clarifying all the contradictions.

Author's response:

Comment accepted.

Author's changes in manuscript:

The Conclusions paragraph was rephrased accordingly.

References:

Alpert, P., Krichak, S. O., Tsidulko, M., Shafir, H., and Joseph, J. H.: A Dust Prediction System with TOMS Initialization, Mon. Weather Rev., 130, 2335–2345, 2002.

Levi Y., Shilo E., and Setter I.: Climatology of a summer coastal boundary layer with 1290-MHz wind profiler radar and a WRF simulation, J. Appl. Meteorol. Climatol., 50, 1815-1826, https://doi.org/10.1175/2011JAMC2598.1, 2011.

Stull R.B.: An introduction to boundary layer meteorology, Kluwer Academic Publishers, the Netherlands, 666 p., 1988.

Uzan, L. and Alpert, P.: The coastal boundary layer and air pollution - a high temporal resolution analysis in the East Mediterranean Coast, The Open Atmospheric Science Journal, 6, 9–18, 2012.

## Author's Response to referee #2:

We wish to thank referee #2 for the constructive comments. Although the referee suggested the article should not be published in its current form, the referee took the time and effort to present a list of comments. The manuscript was intensely reexamined and has gone over a major revision. We thank both the referee and the editor for the opportunity to reply and improve the paper. Our point to point response is given by order of appearance.

Referee's comment:
Although there is no doubt that determining the mixing height is important, the scientific community has done extensive research and progress so far on the daily boundary layer. However, there are still significant problems as well as gaps in the night boundary layer (stable conditions) and in the transitional periods. These periods cannot be omitted in a study when referring to the importance of mixing height in the formulation of concentrations and even more when one of the main initiatives is to designate ceilometers as a correction for NWP. The statement on line 218 is not appropriate for the exclusion of the nighttime period. Also, the methodology applied by the authors for the reliability of PBL estimation from ceilometers data raises many reservations. I personally could not find the value of this research effort. Concluding, I believe that the whole processing of the subject is rather limited, covers a very short period and is of local interest only. Therefore, I do not agree that this study is published in the ACP Journal.

Author's response:
The analysis of the PBL heights from NWP models over diverse terrain and the ability of the regression tool (Eq. 6) to produce adequate corrections presents an interesting study case and a preview of the great potential of ceilometers as a validation and correction tool to discern PBL heights derived by NWP models.

The distribution of ceilometers in Israel is at its first stages. Data for the summer season from as many ceilometers as possible over a heterogeneous area concluded with a time span of two months (August between 2015-2016). Initially, we analyzed the diurnal evolution of the summer PBL height. The models' PBL scheme is based on the bulk Richardson method. Thus, the models estimated the nocturnal surface boundary layer (SBL) as the first model level for all dates examined. Moreover, the ceilometers' detection of the SBL height in ground-level sites was found mainly within the first range gates. At these range gates, a perturbation exists due to the overlap of the emitted laser beam and the receiver's field of view. This constrained our ability to determine the low SBL height of the summer season. Consequently, the research focused on convective daytime hours (09-14 UTC).

Author's changes in manuscript:
The manuscript has gone over a major revision to address the referee's reservations.

Referee's comment:

I wonder if we could perform a similar exercise for an area with restricted characteristics, thus no general applicability. This is the case here, where local flows are developed but there are not taken into consideration. In particular, both sea breeze and/or anabatic winds are expected to develop in this area during the summer period. (1) For this reason, I am not sure what the ceilometer is measuring. (2) For example, at the station of DB just 7 km away from the shore, the PBL depth is measured at 1km. To my knowledge, this is an unrealistic value (too high) under the presence of sea breeze (or IBL). Thus, I wonder if this instrument finally shows the off-shore current of the sea breeze flow.

Author's response:

(1) Local flows are taken into consideration by the models and the ceilometers. While the models simulate the physical parameters generating them (for example, see Fig.1), the ceilometers measure the results of these flows expressed as backscatter signals

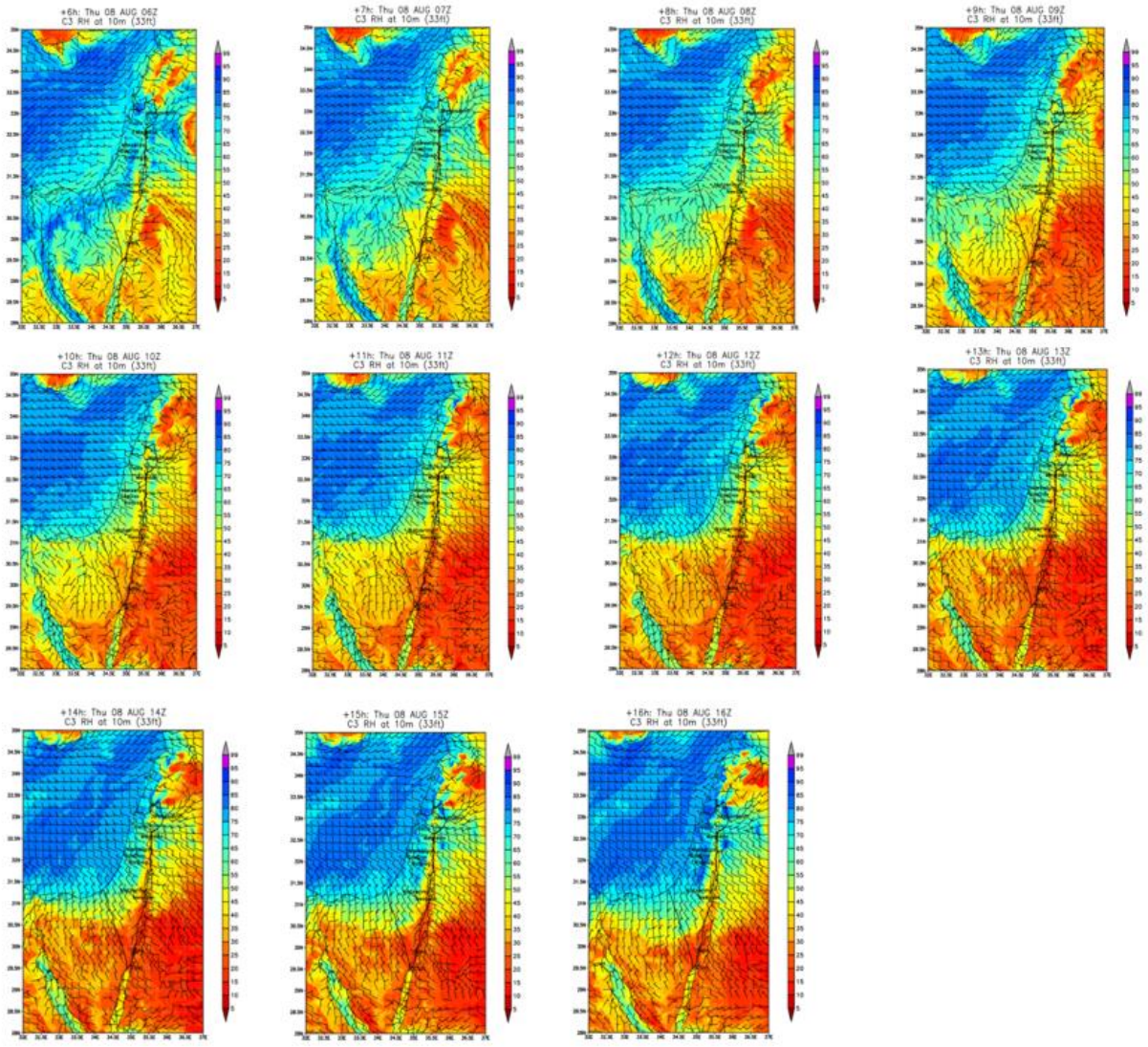


Fig 1. COSMO model maps of RH, wind speed and wind direction over Israel in August 2019 between the hours 07 Z-15 Z (LST=Z-2). Source: Dr. Pavel Khain, Israeli Meteorological Service.

Uzan et al, (2012) studied the ability of the wavelet covariance transform (WCT) method to delineate the evolution of the summer mixed layer height (not the PBL height) based on ceilometers' profile. The results are presented in Fig.2.

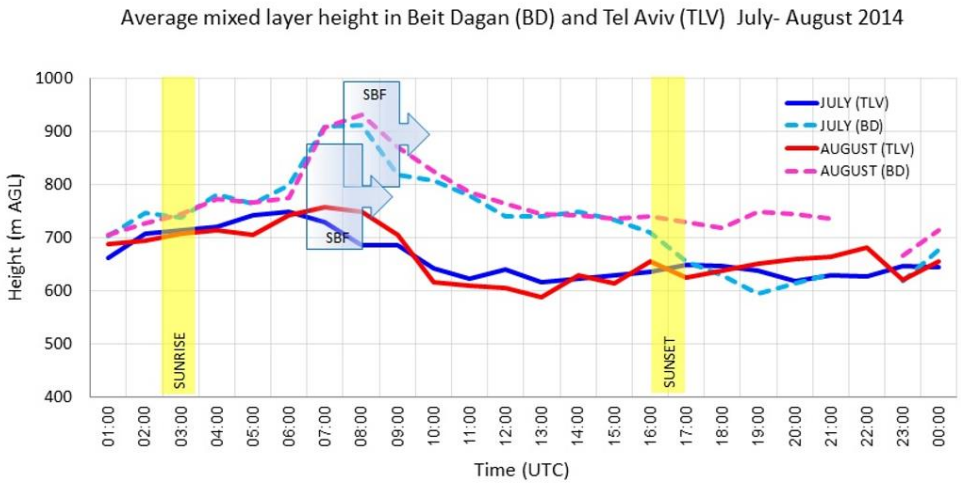


Fig.2 Hourly averaged mixed layer height (MLH) for the east Mediterranean summer season (July – August) 2014. Dashed lines indicated ceilometer measurements in Beit Dagan (BD) and solid lines indicate the measurements in Tel Aviv (TLV) for July (blue and light blue) and August (red and pink). TLV and BD plots are based on 19, 31 days in July and 24, 30 days in August, respectively. Indications of the time of sunrise, sunset and the SBF entrance time are given.

This figure demonstrates the diurnal summer mixed layer height between July-August in 2014. The analysis was carried out by two ceilometer sites: Tel Aviv (50 m from the shoreline, 5 m a.s.l) and Beit Dagan (7.5 km from shoreline, 11 km southeast to Tel Aviv,33 m a.s.l). The ceilometers' measurements succeeded to capture the inflation of the mixed layer height after sunrise followed by subsidence as the sea breeze front prevails. A height difference of 200 m was measured between the two sites at midday. This difference is attributed to the greater distance of Beit Dagan from the shoreline (7.5 km) enabling the convective thermals to develop and inflate the mixed layer height. Tel Aviv site, on the other hand, is practically on the shoreline, therefore the sea breeze promptly surmounts the convective thermals preventing from the mixed layer to inflate. The apparent height difference of the mixed layer height in Beit Dagan in July (dashed blue line) compared to August (dashed pink line) was ascribed to the fact that August was cloudier than July after sunset.

(2) The assertion Beit Dagan PBL height reaches 1000 m a.s.l is based on the following studies:

a) Felix Y, 1994 stated: " The daily inversions over the coast of Israel have been studied by Shaia and Jaffe (1976). Their analysis was based on 10 years of observations of temperature profiles measured by the afternoon radiosonde (1200 UTC) at Bet Dagan (7 km inland from the central coast of Israel). According to their statistics, in 81% of the summer days (June-August), inversions occurred. The base height of most of these inversions was between 500 and 1000 m and their mean thickness was about 400 m.

b) Yuval et al., (2019) evaluated monthly median values of the PBL height (denoted as CBL for midday PBL) as evaluated by the midday Beit Dagan radiosonde profiles, based on the W&W method. Fig. 3 presents the median value of the PBL heights (green line) in August reach 900 m a.s.l.

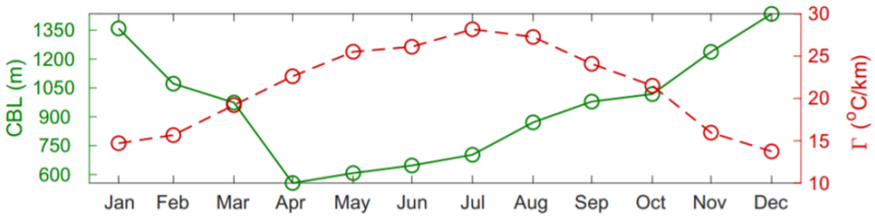


Fig 3. Monthly median values of the PBL height (continuous lines) and the lapse rate Γ (dashed lines) under CBL conditions. The PBL heights were estimated using the W&W method. The lapse rate was calculated between the temperature at the 12th radiosonde reporting level data (24 s from launch, on average at 108 m) and the second level (two seconds, on average 6.2 m).

c) The sea breeze effect is evident by the ceilometers' attenuated backscatter profiles as shown by the figure below depicted from Uzan et al., 2016. Note the Beit Dagan PBL height reaches 1000 m a.g.l.

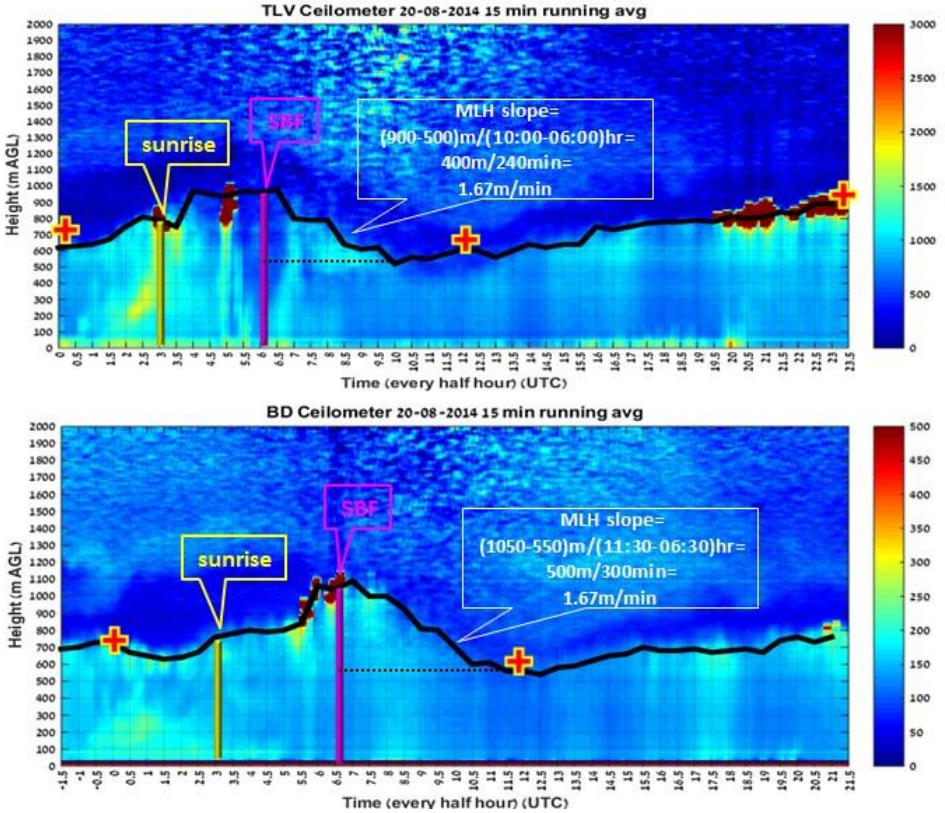


Fig. 4. Mixed layer height (MLH, solid black line) on the 20.08.2014 for Beit Dagan (BD) and Tel Aviv (TLV). The MLH line is laid upon half hourly averaged attenuated backscatter profiles (units 10-6 m-1 sr-1). The BD plot is shifted 2 hours to coincide with UTC time. The plot includes indications of the sunrise (yellow bar) and the sea breeze front (SBF) entrance time (pink bar), MLH evaluation by radiosonde profiles at 0 and 12 UTC (red plus) and calculation of the MLH subsidence rate due to SBF entrance.

Author's changes in manuscript:

The text was rephrased in Sect. 2 (Research area): " On the synoptic scale, the summer is defined by a persistent Persian Trough (either deep, shallow or medium) followed by a

Subtropical High aloft (Felix Y., 1994, Dayan et al., 2002, Alpert et al., 2004). Combined with the sea breeze effect, the average PBL height is found to be quite low. For example, the PBL height in Beit Dagan (33 m a.s.l and 7.5 km east from the shoreline) reaches ~900 m a.s.l after sunrise, and before the entrance of the sea breeze front (Felix Y.,1994, Dayan and Rodinzki, 1999, Uzan et al., 2016, Yuval et al., 2019).".

Referee's comment:

(1) The PBL depth is a non-specific parameter, the definition and estimation of which is not straightforward. The simulated PBL depths are mainly determined, based on the definition that each PBL scheme applies (in this study, no information is provided regarding the PBL parameterization schemes considered by the two models). (2) This also applies between measurements from different instruments (ceilometer and radiosonde) as they do not have the same operating principles. The ceilometer measurements mainly present the mixed PBL that does not always coincide with the simulated PBL depth. (3) On the other hand, has it been taken into account that the radiosonde moves with the flow? As it ascends the measurements do not correspond to the vertical position above the launch point. This is another reason for a possible discrepancy between the radiosonde and the ceilometer measurements.

Author's response:

(1) Comment accepted: Descriptions of the models' PBL parameterization schemes were added to Sect. 3 (IFS and COSMO Models).

(2) We addressed the same methods on the models and radiosonde measurements (the bulk Richardson method and the parcel method). These methods cannot be imposed on the ceilometers' attenuated backscatter profiles, therefore we generated a specific method based on the WCT method, and compared the results to the heights generated by the radiosonde. Results for 33 days (presented in the manuscript in Fig.2 and Table 1) revealed a high correlation between the two instruments (0.93) and low RMSE (97 m).

(3) Radiosonde profiles are retrieved every 10 seconds, corresponding to about every 45 m, reaching 2 km in about 8 minutes. The horizontal displacement of the radiosonde depends on the intensity of the ambient wind speed. In this study, we analyzed the PBL height of midday summer profiles (11 UTC). The average wind speed along these profiles is about 5 m/s (Uzan et al., 2012). Therefore, the horizontal displacement of the radiosonde from its launch position is fairly low and is estimated at about 2.5 km. Moreover, the radiosonde position resolution is defined as 0.01°. The PBL height in Beit Dagan for midday summer is estimated below 1 km (Felix Y.,1994, Dayan and Rodinzki, 1999, Uzan et al., 2016, Yuval et al., 2019). Hence, within an ascending height of 1 km, the change in the radiosonde position will be below 0.01°. This spatial error is in the order of magnitude of the models' grid resolution. Thus, we assert the radiosonde profiles represent the Beit Dagan site and the displacement error of the ascending radiosonde can be neglected

Author's changes in manuscript:

(1) Concise descriptions of the models' schemes were added to Sect. 3 (IFS and COSMO models):

a) IFS PBL parameterization scheme: "The turbulent diffusion scheme represents the vertical exchange of heat, momentum, and moisture through sub-grid scale

turbulence. In the surface layer, the turbulence fluxes are computed using a first-order K-diffusion closure based on the Monin-Obukhov (MO) similarity theory. Above the surface layer, a K-diffusion turbulence closure is used everywhere, except for unstable boundary layers where an Eddy-Diffusivity Mass-Flux (EDMF) framework is applied, to represent the non-local boundary layer eddy fluxes (Koehler et al. 2011)".

b) The COSMO turbulent scheme: "The turbulence scheme, based on Mellor and Yamada (1982) at Level 2.5, uses a reduced second-order closure with a prognostic equation for the turbulent kinetic energy. The transport and local time tendency terms in all the other second-order momentum equations are neglected and the vertical turbulent fluxes are derived diagnostically (Cerenzia I., 2017)".

(2) Sect. 6.1 (Comparison to in-situ radiosonde profiles) was rephrased: " In order to evaluate the daytime PBL heights produced by the models and the ceilometers, the results were compared to the radiosonde's evaluations. Consequently, the investigation was held in Beit Dagan at the time of the midday launch (11 UTC). For this comparison, the ceilometer's 15 s profiles were averaged as half-hour profiles between 10:30-11:00 UTC. COSMO's results referred to the profiles of 10:45 UTC, and IFS estimations were given at 11 UTC. The analysis was carried out for 33 summer days, 13 days from August 2015, and 20 days from Aug 2016. The PBL heights were produced by the same methods: the parcel method (denoted by subscript P) and the bulk Richardson method (denoted by subscript R). These methods require meteorological parameters such as temperature and pressure profiles generated by the models and the radiosonde. Ceilometers, on the other hand, produce only backscatter signals. Therefore, they were analyzed by the WCT method. The results were statistically analyzed by mean error (ME), root mean square error (RMSE), and correlation (R) presented in Fig. 2 and Table 3. Good agreement was found between the ceilometer and the radiosonde (ME = 12 m, RMSE = 97 m, and R = 0.93), although they produced the PBL heights by different methods. ".

(3) Sect. 4.2 (Radiosonde) was rephrased: "The IMS obtains systematic radiosonde atmospheric observations twice daily, at 23 UTC and 11 UTC, adjacent to a ceilometer. Launching is performed in Beit Dagan (32.0 ° long, 34.8 ° lat, 33 m a.s.l), situated 7.5 km east from the shoreline, 11 km southeast to Tel Aviv, 45 km northwest to Jerusalem (Fig.1 and Table 1). The radiosonde, type Vaisala RS41-SG, produces profiles of RH, temperature, pressure, wind speed and wind direction as it ascends. Measurements are retrieved every 10 seconds, corresponding to about every 45 m, reaching 2 km in about 8 minutes. The horizontal displacement of the radiosonde depends on the intensity of the ambient wind speed. The average wind speed along the 11 UTC summer profiles is about 5 m/s (Uzan et al., 2012). Therefore, the horizontal displacement of the radiosonde from its launch position is fairly low and is estimated at about 2.5 km. Moreover, the radiosonde position resolution is defined as 0.01°. As aforementioned, the PBL height in Beit Dagan for midday summer is estimated below 1 km (Dayan and Rodinzki, 1999, Uzan et al., 2016, Yuval et al., 2019). Hence, within an ascending height of 1 km, the change in the radiosonde's horizontal position is under 0.01° which is an order of magnitude from the models' grid resolution. Thus, we assert the radiosonde profiles represent the Beit Dagan site and the displacement error of the ascending radiosonde can be neglected".

Referee's comment:

Therefore, the same criteria should be used for the estimation of both measured and simulated PBL depth. In particular, the same criteria should be applied to the profiles of certain atmospheric parameters, such as temperature, wind and mixing ratio profiles that depict the atmospheric boundary structure. These criteria should not necessarily be the same for all atmospheric conditions. For example, the gradient of potential temperature profile is inadequate to provide the turbulent ABL depth. Therefore, for the comparison with ceilometer, it would be more appropriate to consider the eddy-viscosity simulated profiles or even better the aerosol layering from chemistry transport model simulation.

In particular, under convective conditions, the mixing height determined by ceilometer is strongly related to the aerosol stratification.

Author's response:

We employed the parcel method to evaluate the transition zone between the mixed layer and the free atmosphere, as presented in Fig. 5 from Stull (1988). In this method, the virtual potential temperature at ground level is crucial while the models' lowest grid point is above the surface layer (IFS begins at 10 m a.g.l. and COSMO at 20 m a.g.l.). Therefore, the virtual potential temperature at ground level height (2 m a.g.l) was evaluated by the temperature and dew point temperature (or RH) derived by the models based on the similarity theory.

As explained in the previous comment, we addressed the same methods on the models and radiosonde measurements (the bulk Richardson method and the parcel method). These methods cannot be imposed on the ceilometers' attenuated backscatter profiles, therefore we generated a specific method for the ceilometers' PBL heights evaluations based on the WCT method. To ensure the WCT method addressees the same PBL heights generated by the other methods, we compared the ceilometer's evaluations to the radiosonde's heights. Results for 33 days (presented in the manuscript in Fig.2 and Table 1) revealed a high correlation between the two instruments (0.93) and low RMSE (97 m).

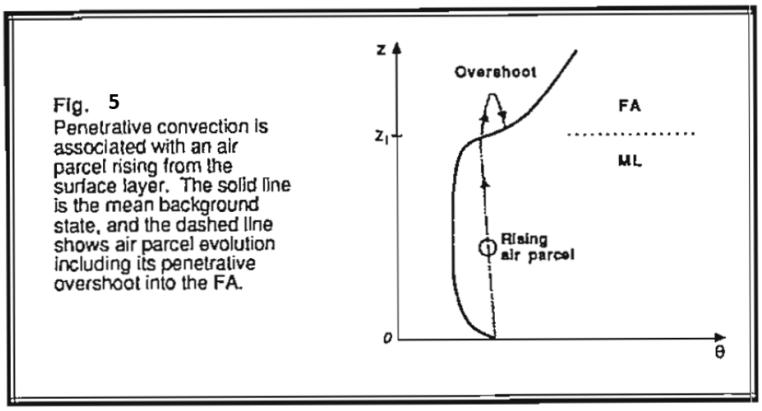


Fig. 5
Penetrative convection is associated with an air parcel rising from the surface layer. The solid line is the mean background state, and the dashed line shows air parcel evolution including its penetrative overshoot into the FA.

(source: Stull, 1988)

Author's changes in manuscript:

No changes were made in the manuscript.

Referee's comment:
How much value does the global model have in such a small analysis to take part in the comparison, especially in a strongly heterogeneous area?
Author's response:
The main goal of the study was to utilize ceilometers as a correction tool for NWP models. Therefore, two types of models were tested, global and regional. The limited ability of the global models to correctly simulate complex terrain was taken into consideration. Therefore, we did not anticipate the significantly large overestimations of IFS over flat grid points under fairly "simple" meteorological conditions characterizing the summer in the East Mediterranean. This disclosed the advantages of the regional model as well as the limitations of the global model in regard to PBL height estimations.
Author's changes in manuscript:
No changes were made in the manuscript.

Referee's comment:
(1) Also, there are several arbitrary statements on the text, without any justification (no measurements of wind speed and direction are provided) or any reference.
(2) For example:
Line 105: "As a result, the average PBL height is comparatively low (~1000 m a.g.l)".
Line 116: "Through the day, the sea breeze circulation steers clockwise and the wind speed is enhanced by the west-north-west synoptic winds".
Line 119: "Due to the large distance (~30-50 km inland), the SBF reaches the eastern elevate complex terrain only in the afternoon (~11-12 UTC).
Line 170:" However, the PBL detection algorithm utilized here (see Sect. 5.3) is based on a significant signal slope, therefore can be determined from uncalibrated ceilometers".
Author's response:
(1) Comment accepted. Moreover, following the comments from referee # 1, the study cases of August 10, 2015, and August 17, 2016, were removed and replaced with the description of a typical case on August 15, 2015, provided with radiosonde profiles of wind, temperature, and relative humidity.
(2) Comment accepted. The whole paragraph was rephrased accordingly and the references were inserted within the text rather than the list given in the previous form.
Author's changes in manuscript:
(1) The study case of August 15, 2015, was provided with radiosonde profiles of temperature, relative humidity, wind speed, and wind direction.
(2) Sect. 2 (Research area) was rephrased in the following manner: "Previous research describes the formation and evolution of the Israeli summer PBL height as a function of the synoptic and mesoscale conditions, as well as the distance from the shoreline, and the topography. Overall, the diurnal PBL height in the summer season may be portrayed in the following manner: After sunrise (~4-5 LST, where LST=UTC+2) clouds initially formed over the Mediterranean Sea are advected eastward to the shoreline. As the ground warms up, the nocturnal surface boundary layer (SBL) dissipates and buoyancy induced convective updrafts to instigate the formation of the sea breeze circulation (Stull, 1988). The entrance of the sea breeze front (SBF) is estimated between 7-9 LST (Felix Y., 1993,

Alpert and Rabinovich-Hadar, 2003, Uzan and Alpert, 2012), depending on the time of sunrise and the different synoptic modes (weak, medium and deep) of the prevailing system – the Persian trough (Alpert et al., 2004). Cool and humid marine air hinder the convective updrafts, thus clouds dissolve and the height of the shoreline convective boundary layer (CBL) lowers by ~250 m (Felix Y., 1993, Felix Y., 1994, Levi et al., 2011, Uzan and Alpert, 2012). Further inland, the convective thermals continue to inflate the CBL (Hashmonay et al., 1991, Felix, 1993, Lieman, R. and Alpert, 1993) while the sea breeze circulation steers clockwise and wind speed is enhanced by the west-north-west synoptic winds (Neumann, 1952, Neumann, 1977, Uzan and Alpert, 2012). By noontime (~11-13 LST), the sea breeze and the synoptic wind merge and produce maximum wind speeds which suppress the CBL (Uzan and Alpert, 2012). In the afternoon (~13-14 LST), the SBF reaches ~30-50 km inland to the eastern elevated complex terrain (Hashmonay et al., 1991, Lieman, R. and Alpert, 1993). At sunset (~18-19 LST), as the insolation diminishes, the potential energy of the convective updrafts weakens and the CBL height drops (Dayan and Rodnizki, 1999). After sunset, the CBL finally collapses and a residual layer (RL) is formed above the SBL (Stull, 1988). As the ground cools down, the high humidity and low RL create low condensation levels which produce shallow evening clouds".

Referee's comment:

Line 203-Does the bulk Richardson refers to a certain height or layer?

Author's response:

The bulk Richardson method refers to a certain layer in the models and to a specific height in the radiosonde profiles.

Author's changes in manuscript:

Sect 5.1 (The bulk Richardson number method) was rephrased as follows:" The IFS model defines the PBL height as the lowest height level at which the Rb (Eq. 1) reaches a critical threshold of 0.25 (ECMWF-IFS documentation – Cy43r3, Part IV: Physical Processes, July 2017). The PBL height is distinguished by scanning the bulk Richardson results from the surface upwards. When the PBL height is found between two levels of the model, it is determined by linear interpolation. Radiosonde's profiles were analyzed in the same manner by a $R_b$ threshold of 0.25 to detect a specific height rather than a certain layer.

COSMO estimates the $R_b$ based on the dynamic conditions of the first four levels (10, 34.2, 67.9, 112.3 m a.g.l.) signified by a threshold of 0.33 for stable conditions and 0.22 for unstable ones. If no level is found, then a missing value is assigned for the PBL height".

Referee's comment:

Lines 265-end of this paragraph. I am confused.

Author's response:

The end of the paragraph states: "However, as previously mentioned, our algorithm denotes the PBL height as the top of the shallow cloud (Stull, 1988)". We assume the confusion regards the term "cloud top". We agree with the referee this definition is confusing within the context

it was used and apologize for the misunderstanding we have caused. The term was changed given the explanation as follows:

In this research, we employed the wavelet covariance transform (WCT) method on the ceilometers' backscatter profiles. The principle of this method is to calculate the derivatives between measuring points along with the backscatter profile. The highest derivative implies a profound difference in the atmospheric aerosol content. On clear days, this difference occurs as the transmitted light exits the well-mixed layer and enters the stable layer above. In the presence of clouds, the highest values are retrieved at cloud base height which is considered as the mixed layer height. The cloud top denotes the bottom height of the free atmosphere (see Fig.6 from Stull, 1988).

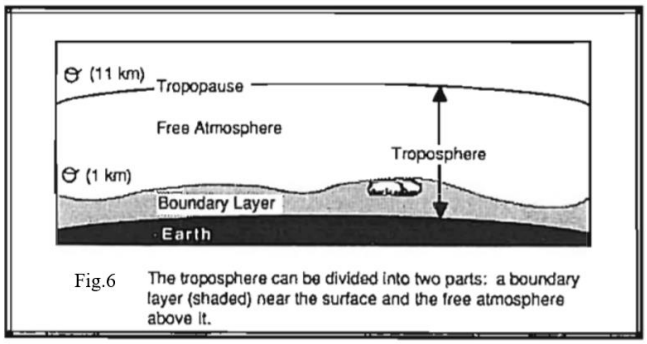


Fig.6 The troposphere can be divided into two parts: a boundary layer (shaded) near the surface and the free atmosphere above it.

(Source: Stull, 1988)

Therefore, in order to generate a consistent definition of the PBL height by the WCT method, our algorithm seeks the height of the transition zone in the presence of clouds as well. This height is defined here as the highest measuring point of a cloud above the cloud base height. Even though the summer clouds are relatively shallow (~ 500 m thickness based on observations, see example in Fig.5 and Fig.6 below), there is no guarantee the algorithm detects the actual cloud top. Therefore, to prevent misinterpretations, the phrase "cloud top" was omitted and clarified as the highest measurement point of a cloud above a cloud base height.


Fig 7. IMS photograph of the sky over Beit Dagan site on August 2, 2019, at 8 UTC presenting typical shallow cumulus clouds.

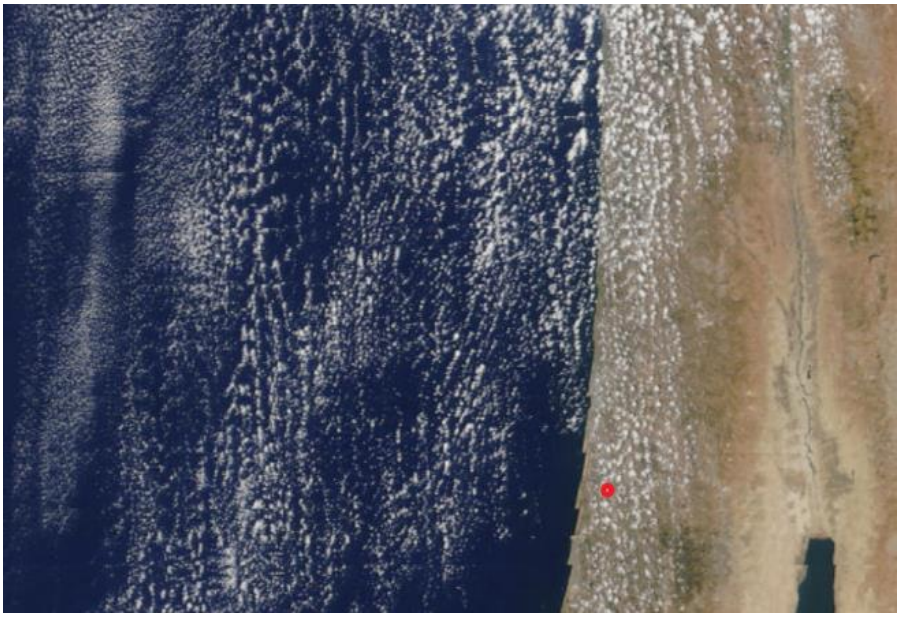

Fig 8. Terra-MODIS 250 m resolution picture over Israel on August 2, 2019, at 8 UTC. Beit Dagan site is indicated by a red dot. Adapted from @NOAA- EARTHDATA.

Author's changes in manuscript:

" When clouds are present (mainly summer shallow cumulous), the algorithm defines the highest measurement point of a cloud (above the cloud base height) as the height where the signal counts decrease to the amount retrieved by background values. This signifies the ceilometer's identification of the entrainment zone (Stull, 1988)".

References:

Bruine, M., Apituley, A., Donovan, D.P., Klein Baltink, H. and de Haij, M.J.: Pathfinder: applying graph theory to consistent tracking of daytime mixed layer height with backscatter lidar, Atmospheric Measurement Techniques, 10, 1893–1909. https://doi.org/10.5194/amt-10-1893-2017, 2017.

Cerenzia I., Challenges and critical aspects in stable boundary layer representation in numerical weather prediction modeling: diagnostic analyses and proposals for improvement, Ph.D. thesis, University of Bologna, 2017.

Feliks, Y: An analytical model of the diurnal oscillation of the inversion base due to sea breeze, J. Atmos. Sci., 51, 991-998,1994.

Kotthaus, S. and Grimmond, C.S.B.: Atmospheric boundary-layer characteristics from ceilometer measurements. Part 1: a new method to track mixed layer height and classify clouds, Q J R Meteorol. Soc.,144 (714), 1525–1538, https://doi.org/10.1002/qj.3299, 2018.

Sokół, P., Stachlewska, I., Ungureanu, I. and Stefan, S.: Evaluation of the boundary layer morning transition using the CL-31 ceilometer signals, Acta Geophysica, 62, 367–380. https://doi.org/10.2478/s11600-013-0158-5, 2014.

Stull R.B.: An introduction to boundary layer meteorology, Kluwer Academic Publishers, the Netherlands, 666 p., 1988.

Uzan, L., Egert, S., and Alpert, P.: Ceilometer evaluation of the eastern Mediterranean summer boundary layer height – first study of two Israeli sites, Atmos. Meas. Tech., 9, 4387–4398, https://doi.org/10.5194/amt-9-4387-2016, 2016.

Yuval, Dayan, U., Levy, I., & Broday, D. M**:** On the association between characteristics of the atmospheric boundary layer and air pollution concentrations, Atmospheric Research, doi.org/10.1016/j.atmosers.2019.104675, 2019.

**********

**Author's comment:**

Following the referees' comments, we repeatedly examined our datasets and the methods. We found that the equations of the virtual temperature (Eq.1) and the virtual potential temperature (Eq.2) employed values of Rd/Cp = 287/1004 (~ = 0.28586), and surface pressure of $P_0$ =1000 mb for the radiosonde data, while in the models, these factors were defined as Rd/Cp = 0.263, $P_0$ = 1013.15 mb**.** Therefore, we decided to transform all factors to the same values of Rd/Cp = 287/1004, $P_0$ = 1000 mb. Essentially, this altered the models' results based on the parcel method (see changes in Tables 3-5 and Fig. 2 below). It did not change the results of the correction equation or the conclusions of the research.

$$(1)\ T_v = \frac{T}{1-\frac{e}{P}(1-\varepsilon)} \qquad (2)\ \theta_v = T_v\left(\frac{P_0}{P}\right)^{\frac{Rd}{Cp}}$$

Before

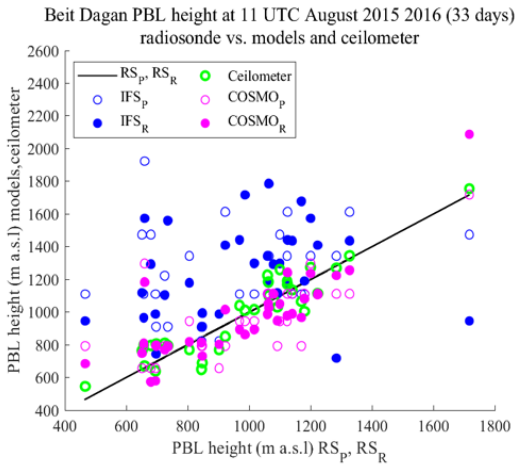


After

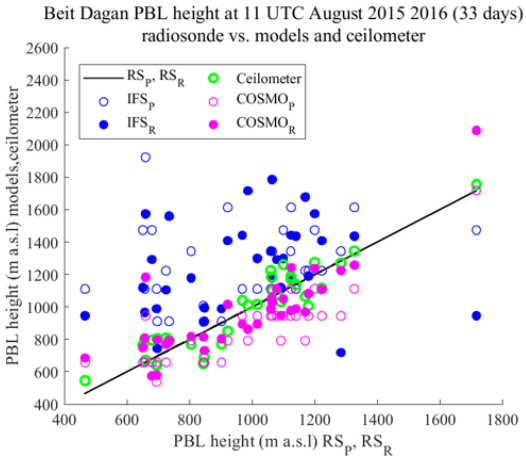


Fig 2. PBL heights over Beit Dagan site on 33 summer days (13 days on August 2015 and 20 days on August 2016), generated by the bulk Richardson method for IFS model ($IFS_R$, blue solid circles), COSMO model ($COSMO_R$, pink solid circles), and Beit Dagan radiosonde profiles ($RS_R$, black line). PBL heights generated by the parcel method for the IFS model ($IFS_P$, open blue circles), COSMO model ($COSMO_P$, open pink circles), and Beit Dagan radiosonde profiles ($RS_P$, same black line as $RS_R$, the results are identical). PBL heights derived from the Beit Dagan ceilometer produced by the WCT method (green circles). Results for August 17, 2016, are indicated by a circle.

Table 3. Statistical analysis of the Beit Dagan PBL heights on 33 summer days (13 days in August 2015 and 20 days in August 2016) from IFS and COSMO models by the bulk Richardson method ($IFS_R$, $COSMO_R$), the parcel method ($IFS_P$, $COSMO_P$) and the WCT method for the adjacent ceilometer. The PBL heights were compared to those derived from Beit Dagan radiosonde by either the parcel or bulk Richardson methods (see Fig 2).

| PBL detection | $IFS_R$ | $IFS_P$ | $COSMO_R$ | $COSMO_P$ | Ceilometer |
|---|---|---|---|---|---|
| Mean Error (m) | 274 | 249 (271) | -3 | -17 (-106) | 12 |
| RMSE (m) | 432 | 409 (411) | 152 | 179 (176) | 97 |
| R | 0.18 | 0.18 (0.21) | 0.83 | 0.73 (0.83) | 0.93 |
| Mean PBL (m a.s.l) | 1250 | 1225 (1247) | 973 | 959 (869) | 989 |
| Std PBL (m) | 274 | 256 (245) | 273 | 229 (222) | 259 |

*New results are given in brackets.

Table 4. Root mean square errors of PBL heights from five sites on 13 summer days (Fig. 4), derived by IFS and COSMO models by the bulk Richardson method ($IFS_R$, $COSMO_R$) and the parcel method ($IFS_P$, $COSMO_P$). The PBL heights were compared to the heights measured by the Beit Dagan ceilometer.

| Site | $IFS_R$ | $IFS_P$ | $COSMO_R$ | $COSMO_P$ |
|---|---|---|---|---|
| Ramat David | 173 m | 191 (180) m | 247 m | 241 (232) m |
| Tel Aviv | 276 m | 465 (498) m | 203 m | 183 (182 ) m |
| Beit Dagan | 405 m | 569 (569) m | 235 m | 234 (171) m |
| Weizmann | 214 m | 274 (339) m | 175 m | 145 (209) m |
| Jerusalem | 351 m | 368 (285) m | 251 m | 273 (179) m |

*New results are given in brackets.

Table 5. Same as in Table 3 but for mean errors.

| Site | $IFS_R$ | $IFS_P$ | $COSMO_R$ | $COSMO_P$ |
|---|---|---|---|---|
| Ramat David | -31 m | 30 (0) m | -26 m | 0 (-12) m |
| Tel Aviv | 234 m | 376 (422) m | 19 m | -35 (-35) m |
| Beit Dagan | 332 m | 497 (497) m | 12 m | -9 (-55) m |
| Weizmann | 114 m | 218 (280) m | 16 m | -42 (-42) m |
| Jerusalem | 298 m | 327 (243) m | -6 m | 29 ( -1) m |

*New results are given in brackets.

**********

## A list of relevant changes made in the manuscript:

1. Abstract- slightly changed to emphasize the goal and advantage of the research.
2. Introduction – additional text on the benefits of ceilometers as a research tool.
3. Research area- the description was elaborated and rephrased according to the relevant references.
4. IFS and COSMO models- the parameterization schemes were added.
5. Instruments- additional information regarding the radiosonde and ceilometers.
6. Methods- the section was rephrased in a concise manner.
7. Results- the study cases were changed according to the referees' comments.
8. Summary and conclusions - rephrased.

# Ceilometers as planetary boundary layer height detectors and a corrective tool for ECMWF and COSMO NWP models

Leenes Uzan[1,2], Smadar Egert[1], Pavel Khain[2], Yoav Levi[2], Elyakom Vladislavsky[2], Pinhas Alpert[1]

[1] Department of Geosciences[1] Porter School of the Environment and Earth Sciences, Raymond and Beverly Sackler Faculty of Exact Sciences,
Tel-Aviv University, Tel Aviv, 6997801, Israel.
[2] The Israeli Meteorological Service, Beit Dagan, Israel.

Correspondence to: Leenes Uzan (Leenesu@gmail.com)

## Abstract

The growing importance of the planetary boundary layer (PBL) height detection is apparent in various fields, from air pollution analysis to weather prediction. In recent years micro-lidars such as Here, we demonstrate the capability of ceilometers have been recognized as an efficientto serve as a validation tool for such measurements. Here, the models' PBL height estimations. The study focused on the daytime summer PBL height is measured by eight ceilometers throughout Israel, along with radiosonde profilesheights over a heterogeneous area. Height values from two numerical weather models, the global IFS model, and the regional COSMO model. The analysis focused on three PBL height were evaluated against actual measurements from a radiosonde and eight ceilometers. The evaluation methods: of the PBL heights was attained by the bulk Richardson method, and the parcel method, and the . The ceilometers' backscatter profiles were analyzed by the wavelet covariance transform method. The bestA comparison of the PBL heights at 11 UTC on 33 summer days in Beit Dagan radiosonde launch site revealed a good agreement between the PBL heights derived from a single radiosonde site on 33 summer days was found byand the adjacent ceilometer (mean error = 12 m, RMSE = 97 m). Spatial analysis of the PBL heights derived from the models on 13 days in referencecompared to results from five ceilometer measurement sites revealedshowed COSMO evaluations by the bulk Richardson method ($COSMO_R$) produced the bestgood results for both flat (mean error = 19 m, RMSE = 203 m) and elevated terrain (mean error = -6 m, RMSE = 251 m). To improvecorrect $COSMO_R$ resultsheight estimations, a regression tool was assimilatedgenerated based on the PBL height difference between $COSMO_R$ and eight ceilometers. from diverse sites. The regression is based onindependent predictor variables are

the ~~altitude~~topography and the distance from the shoreline~~ for eight ceilometer sites.~~. The correction factors are implemented on the $COSMO_R$ PBL height results.

## 1. Introduction

In this era of heavy industrialization, the need to mitigate the detrimental effects of air pollution exposure is unquestionable. However, in order to regulate and establish environmental thresholds, a comprehensive understanding of the air pollution dispersion processes is necessary. One of the key meteorological parameters governing air pollution dispersion is the planetary boundary layer (PBL) height. The PBL height is classified as the first level of the atmosphere which dictates the vertical dispersion extent of air pollution (Stull, 1988). Consequently, the concentration level of air pollution varies depending on the height of the PBL.

~~Previous studies~~Applicable evaluation of PBL heights can be derived either by actual measurements or estimations based on numerical weather prediction (NWP) models. On the one hand, NWP models, such as regional models, provide high temporal and spatial data resolution beyond the capability of actual measurements. On the other, they are based on mathematical equations with initial assumptions and boundary conditioned set beforehand. Hence, the models' products require a systematic validation tool based on actual measurements.

There are two main PBL height measurement methods: in-situ radiosonde launches and remote sensings such as lidars and profilers. Unfortunately, radiosonde launches are costly as successive measurements. Profilers and sophisticated lidars produce high temporal resolution profiles but are limited in space. Moreover, certain meteorological conditions may reduce their performance, such as precipitation for radio acoustic sounding system profilers (Uzan et al., 2012) and dust storms for Raman lidars (Mamouri et al., 2016).

These limitations have led several research groups to successfully utilized ceilometers - single wavelength cloud base height detectors, as a means to recognize and determine the PBL height (Eresmaa et al., 2006, Haeffelin and Angelini, 2012, Wiegner et al., ~~2014, Kotthaus and Grimmond, 2018). Over the past decade, however, the ceilometer has become recognized as a significant remote sensing tool, and is no longer perceived merely as a cloud base height detector (Wiegner et al., 2014).~~2014). Ubiquitous in airports and meteorological service centers worldwide, ceilometers ~~are valuable and effective instruments which produce high resolution~~

~~aerosol backscatter profiles (~~obtain a wide spatial resolution per lidar (for further information see TOPROF of COST Action ES1303 and E-PROFILE of the EUMETNET Profiling Program). They produce high temporal resolution profiles about every 15 s~~,~~ and every 10 m, up to several km~~). ~~, retrieved as attenuated backscatter signals. The ceilometers are low cost, easy to maintain, and operate continuously unattended under diverse meteorological conditions (Kotthaus and Grimmond, 2018). These qualities reflect their advantages over high-cost, multi-wavelength sophisticated lidars, ~~which~~that require surveillance, calibration procedures, and careful maintenance. Hence, they are limited in ~~amount~~space and operational time (Mamouri et al., ~~2016). ~~2016) and cannot achieve the spatial and temporal measurements coverage essential to validate the PBL heights generated by NWP models.

Gierens et al (2018) established a PBL height algorithm applied to the ceilometers' profiles. The PBL height was classified according to daytime convective mixing and ~~a ~~nighttime stable surface layer accompanied by a residual layer aloft. Their research~~,~~ was conducted in northwestern South Africa ~~during~~from October 2012–August 2014, showed good agreement with ERA-Interim reanalysis.

Another operational PBL height detection method was established by Collaud Coen et al. (2014). Their study, implemented on a two-year data set for two rural sites located on the Swiss plateau, included several remote sensing instruments (wind profiler, Raman lidar, microwave radiometer) and several algorithms (the parcel method, the bulk Richardson number method, surface-based temperature inversion, and aerosol or humidity gradient analysis). The results were validated against radio-sounding measurements and compared to the ~~numerical weather prediction (~~NWP~~)~~ model COSMO-2 (2.2 km resolution). ~~The ~~In this research, the authors recommended using ceilometers ~~for~~as complementary ~~measurement data~~measurements of the residual layer~~ alone~~.

Ketterer et al. (2014) focused on the development of the PBL in the Swiss Alps by an adjacent ceilometer, wind profiler, and in-situ continuous aerosol measurements. The ceilometer's profiles were analyzed by the gradient and STRAT-2D algorithms. Good agreement was found between the PBL height derived from the ceilometer and wind profiler during the daytime and under cloud-free conditions. However, comparisons to the calculated PBL heights from the COSMO-2 model yielded low correlations.

Despite this extensive research, so far, scarce attention has been paid to designate ceilometers as a correction tool for NWP ~~(Szintai and Kaufmann, 2007, Kuhn et al, 2018). In ~~PBL height

assessments. The main goal of this study ~~we analyze~~was to evaluate the estimations of the models for the daytime summer PBL ~~height~~heights over complex terrain ~~of Israel derived from NWP models and corrected by~~by comparing the results against remote sensing measurements from ~~eight~~ ceilometers. ~~Models and instruments are described in Sect.~~ Ceilometers~~3 and Sect. 4, respectively, and PBL height detection methods are presented in Sect. 5. The results of NWP models as compared to in-situ radiosonde and ceilometer measurements are presented in Sect. 6. Finally, conclusions are drawn in Sect. 7 regarding the capabilities of NWP models and the evolution of the daytime PBL height over Israel.~~

~~**2. Research area**~~

~~Located in the East Mediterranean, Israel obtains systematic radiosonde atmospheric observations twice daily by the Israeli Meteorological Service (IMS) in Beit Dagan. Hence, the opportunity to widen the scope of atmospheric observation by means of affordable, low cost devices such as ceilometers is of utmost interest. This study was conducted using eight ceilometers deployed at diverse sites (Fig.1, Table 1), from the Mediterranean climate in north to the arid climate of the southern desert.~~

~~Essentially, as ceilometers~~ produce aerosol backscatter profiles, therefore, the evaluation of the PBL height during precipitation episodes becomes difficult (Collaud et al. 2014, Ketterer et al. 2014, Kotthaus & Grimmond 2018). Accordingly, ~~in~~ this study~~, we~~ focused on the summer season.

The research area and time period are explained in Sect. 2. The models and instruments applied are described in Sect. 3 and Sect. 4, respectively. The PBL height detection methods are presented in Sect. 5. Results of NWP models compared to in-situ radiosonde and ceilometer measurements are presented in Sect. 6. Finally, summary and conclusions are drawn in Sect. 7 regarding the capabilities of NWP models and the evolution of the daytime summer PBL height over Israel.

## 2. Research area

~~, with~~ Located in the East Mediterranean, Israel obtains a heterogeneous research area in comparatively short distances, comprised of mountains and valleys in the north and the east, a coastline in the west and a desert in the south. This provides a range of meteorological conditions, from the humid climate on the coast to the arid south.

The Israeli summer season (June-September) is characterized by dry weather (no precipitation~~,~~), high relative humidity (RH~~,~~) - up to 80% in midday in the shoreline~~,~~ (Israeli Meteorological Service -IMS weather reports~~),~~) and sporadic shallow ~~cumulous~~cumulus clouds. On the synoptic scale, the summer is ~~characterized between June-September~~defined by a persistent Persian Trough (either deep, shallow or medium) followed by a Subtropical High aloft (Felix Y., 1994, Dayan et al., 2002, Alpert et al., 2004). ~~As a result~~Combined with the sea breeze, the average PBL height is ~~comparatively~~ found to be quite low ~~(~ 1000~~. For example, the average summer PBL height in Beit Dagan (33 m a.s.l and 7.5 km east from the shoreline) reaches ~900 m a.g.l~~).~~

~~Comprehensive research~~ after sunrise, and before the entrance of the ~~Israeli summer PBL (Neumann, 1952, Neumann, 1977, Dayan et al., 1988, Lieman, R. and Alpert, 1993, Hashmonay et al., 1991,~~ sea breeze front (Felix~~, 1993, Felix,~~ Y.,1994, Dayan and ~~Rodnizki~~Rodinzki, 1999, ~~Dayan~~Uzan et al., 2016, Yuval et al., ~~2002, Alpert and Rabinovich-Hadar, 2003, Felix, 2004, Levi et al., 2011, Uzan and Alpert, 2012, Uzan~~2019). Summer dust outbreaks in the eastern Mediterranean are quite rare (Alpert and Ziv 1989, Alpert et al., 2000) therefore, they were not addressed here, especially in the height levels below 1 km (Alpert et al ~~2016) is generally described in~~ ., 2002).

Previous research describes the formation and evolution of the Israeli summer PBL height as a function of the synoptic and mesoscale conditions, as well as the distance from the shoreline, and the topography. Overall, the diurnal PBL height in the summer season may be portrayed in the following manner: After sunrise (~~2-3-~~4-5 LST, where LST=UTC+2) clouds initially formed over the Mediterranean Sea are advected eastward to the shoreline. As the ground warms up, the nocturnal surface boundary layer (SBL) dissipates and buoyancy induced convective updrafts instigate the formation of the sea breeze circulation~~.~~ (Stull, 1988). The entrance of the sea breeze front (SBF) is estimated between ~~5-8 UTC,~~7-9 LST (Felix Y., 1993, Alpert and Rabinovich-Hadar, 2003, Uzan and Alpert, 2012), depending on the time of sunrise and the different synoptic modes of the prevailing ~~synoptic~~ system~~.~~ – the Persian Trough (Alpert et al., 2004). Cool and humid marine air hinder the convective updrafts~~, thus clouds~~. Clouds dissolve and the height of the shoreline convective boundary layer (CBL) lowers by ~250 m~~. All the while, further~~ (Felix Y., 1993, Felix Y., 1994, Levi et al., 2011, Uzan and Alpert, 2012). Further inland, the convective thermals continue to inflate the CBL~~. Through the day, the~~ (Hashmonay et al., 1991, Felix, 1993, Lieman, R. and Alpert, 1993). The sea breeze circulation steers clockwise and the PBL wind speed is enhanced by the west-north-west

synoptic winds~~.~~ (Neumann, 1952, Neumann, 1977, Uzan and Alpert, 2012). By noontime (~~9-11 UTC) this combination achieves~~ 13 LST) maximum wind speeds~~, suppressing~~ further suppress the CBL ~~even lower. Due to the large distance (~30-50 km inland~~(Uzan and Alpert, 2012). In the afternoon (~13-14 LST), the SBF reaches ~30-50 km inland to the eastern elevated complex terrain ~~only in the afternoon (~ 11-12 UTC).~~(Hashmonay et al., 1991, Lieman, R. and Alpert, 1993). At sunset (~~16-17 UTC~~18-19 LST), as the insolation diminishes, the potential energy of the convective updrafts weakens ~~therefore~~and the CBL height drops~~.~~ (Dayan and Rodnizki, 1999). After sunset, the CBL finally collapses and a residual layer (RL) is formed above ~~a~~the SBL~~. The combination of a typical summer low RL and increased~~ (Stull, 1988) as the ground cools down. High humidity ~~(due to ground cooling), produces a~~and low RL create low condensation ~~level which forms~~levels and shallow evening clouds~~.~~ are produced.

## 3. IFS and COSMO Models

The ~~PBL short range forecasts were produced by~~IMS utilizes two operational models ~~used operationally by the IMS: the ECMWF (~~: The European Centre for Medium-range Weather Forecasts (ECMWF) Integrated Forecast System (IFS) global model, and the ~~regional COSMO (~~consortium for small-scale ~~modelling)~~ modeling (COSMO) regional model ~~(~~. Details of each model are given in Table 2~~).~~.

COSMO (~2.5km resolution) has been running at the IMS over the Eastern Mediterranean domain (25-39 E/26-36 N) since 2013, with boundary and initial conditions from IFS. It is based on the primitive thermo-hydrodynamic equations describing non-hydrostatic compressible flow in a moist atmosphere (Steppeler et al., 2003, Doms et al., 2011, Baldauf et al., 2011). Its vertical extension reaches 23.5 km (~30 hPa) with 60 vertical ~~model~~ levels. The model runs a two-time level integration scheme based on a third order of the Runge–Kutta method and a fifth-order of the upwind scheme for horizontal advection. Unlike IFS, the deep convection parametrization is switched off, while only the shallow convection is ~~parametrized (Tiedtke, 1989). COSMO has been running at the IMS over the Eastern Mediterranean (EM) (domain 25-39 E/26-36 N) with the same resolution since 2013, with boundary and initial conditions from IFS. In 2015, the IFS horizontal resolution was ~13 km and 137 vertical levels. In 2016, the horizontal resolution was improved upon to reach ~10 km.~~ parameterized (Tiedtke, 1989). The turbulence scheme, based on Mellor and Yamada (1982) at Level 2.5,

uses a reduced second-order closure with a prognostic equation for the turbulent kinetic energy. The transport and local time tendency terms in all the other second-order momentum equations are neglected and the vertical turbulent fluxes are derived diagnostically (Cerenzia I., 2017).

~~The resolution of all models influences their topography, causing the latter to vary from the real heights. Thus, in our research, which relied on the two aforementioned models, the PBL heights were corrected to the actual ones above sea level (Table 1).~~

~~IFS profiles were limited to~~ The resolution of IFS has improved from ~13 km in 2015 to ~10 km in 2016 and consists of 137 vertical levels. Its turbulent diffusion scheme represents the vertical exchange of heat, momentum, and moisture through sub-grid scale turbulence. In the surface layer, the turbulence fluxes are computed using a first-order K-diffusion closure based on the Monin-Obukhov (MO) similarity theory. Above the surface layer, a K-diffusion turbulence closure is used everywhere except for unstable boundary layers where an Eddy-Diffusivity Mass-Flux (EDMF) framework is applied to represent the non-local boundary layer eddy fluxes (Koehler et al. 2011).

The spatial resolution of the models affects their ability to refer to the actual topography rather than a smoothed grid point. Therefore, the models' results were corrected by the actual ground base heights for each measurement site (Table 1).

Concerning the time resolution, IFS produced hourly ~~resolution,~~results while COSMO generated profiles every 15 ~~minutes~~min. To compare ~~COSMO's~~ PBL heights from both models, a series of trials ~~were performed to find the correct representation of hourly values as~~disclosed that COSMO profiles of the last 15 ~~minutes~~min within an hour~~.~~ best represent the hourly values of IFS.

## 4. Instruments

### 4.1 Ceilometers

Vaisala ceilometers type CL31~~ are,~~ commonly deployed worldwide,~~ and~~ are the main research tool in this study. CL31 is a pulsed, elastic micro-lidar, employing an Indium Gallium Arsenide (InGaAs) laser diode transmitter of a near~~-~~infrared~~ (NIR)~~ wavelength of 910 nm ±10 nm at 25˚C with a high pulse repetition rate of 10 kHz every two seconds (Vaisala ceilometer CL31 user's guide: http://www.vaisala.com). The backscatter signals are collected by an avalanche

photodiode (APD) receiver and designed as attenuated backscatter profiles at intervals of 2-120 s (determined by the user).

~~Following Weigner et al., (2014), it should be noticed that as single wavelength lidars, ceilometers cannot produce any information on the microphysical properties of the atmospheric aerosol content. Therefore, the assessment of their optical depth is impossible. On the other hand, by employing a NIR wavelength, a pronounced change of the attenuated backscatter profile is mainly attributed to variations in the aerosol content, providing more reliable indications for clouds and atmospheric layers.~~

In this study, CL31 ceilometers were ~~located in diverse sites (Fig.1),~~applied with the exception of ceilometer CL51~~, which was stationed~~ in the Weizmann Institute~~.~~ (Fig.1, Table 1). CL51 consists of a higher signal and signal-to-noise ratio, hence the backscatter profile measurement reaches up to 15.4 km~~.~~ compared to 7 km of CL31.

One drawback is that calibration procedures were nonexistent in all sites, and in most cases, maintenance procedures (cleaning of the ceilometer window) were not regularly carried out, with the exception of the IMS Beit Dagan ceilometer. ~~However, the PBL detection algorithm utilized here (see Sect. 5.3) is based on a significant signal slope, therefore can be determined from uncalibrated ceilometers.~~Nevertheless, the PBL height detection is based on a pronounced change of the attenuated backscatter profile. This change is attributed to variations in the aerosol content providing indications for both clouds and atmospheric layers. Therefore, the limitation of a single wavelength within the spectral range of water vapor absorption does not affect this type of detection. In order to derive the backscatter coefficient from ceilometer measurements, signal calibrations and water vapor corrections are necessary (Weigner et al., 2014, Wiegner and Gasteiger, 2015).

The ~~diurnal PBL measured by the~~ ceilometers ~~is the CBL at daytime and RL at nighttime (Ketterer et al., 2014).~~produce profiles every 15 or 16 sec (Table 1). In ~~this research,~~order to compare them to the models' hourly results (Sect. 3), they were averaged to half-hour ones, whereas the second half-hour profile within each hour was chosen for the comparison process.

The nocturnal SBL ~~was not investigated due to~~ heights in ground-level ceilometer sites were detected mainly within the ceilometers' first range gates. At these heights, a constant perturbation ~~within the first range gates at~~ existed due to the overlap ~~height between~~of the

emitted laser beam and the receiver's field of view. This fact limited our capability to determine the low SBL height of the summer season and heightened our decision to focused on daytime CBL heights. Detailed information regarding the manufactural and technical properties of ceilometers involved in this research~~,~~ are given in Uzan et al. (2018). ~~To compare the hourly results of the models (Sect. 3), the ceilometers' 15 seconds profiles were averaged to half-hour ones, whereas the second half-hour profile within each hour was chosen.~~

## 4.2 Radiosonde

~~Radiosonde (RS) type Vaisala RS41-SG is launched twice daily at 23 UTC and 11 UTC by the IMS in the Beit Dagan site, adjacent to the ceilometer. The radiosonde generates profiles of RH, temperature, and pressure, as well as wind speed and wind direction. The PBL height was determined by profiles retrieved every 10 seconds at ~ 45 m height resolution.~~

The IMS obtains systematic radiosonde atmospheric observations twice daily, at 23 UTC and 11 UTC, adjacent to a ceilometer. Launching is performed in Beit Dagan (32.0 ° long, 34.8 ° lat, 33 m a.s.l), situated 7.5 km east from the shoreline, 11 km southeast to Tel Aviv, 45 km northwest to Jerusalem (Fig.1 and Table 1). The radiosonde, type Vaisala RS41-SG, produces profiles of RH, temperature, pressure, wind speed and wind direction as it ascends. Measurements are retrieved every 10 seconds, corresponding to about every 45 m, reaching 2 km in about 8 minutes. The horizontal displacement of the radiosonde depends on the intensity of the ambient wind speed. The average wind speed along the 11 UTC summer profiles is about 5 m/s (Uzan et al., 2012). Therefore, the horizontal displacement of the radiosonde from its launch position is fairly low and is estimated at about 2.5 km. Moreover, the radiosonde position resolution is defined as 0.01°. As aforementioned, the PBL height in Beit Dagan for midday summer is estimated below 1 km (Dayan and Rodinzki, 1999, Uzan et al., 2016, Yuval et al., 2019). Hence, within an ascending height of 1 km, the change in the radiosonde's horizontal position is under 0.01° which is an order of magnitude from the models' grid resolution. Thus, we assert the radiosonde profiles represent the Beit Dagan site and the displacement error of the ascending radiosonde can be neglected.

## 5. Methods

### 5.1 The bulk Richardson number method

Both COSMO and IFS schemes calculate the PBL height usingby the bulk Richardson number method ($R_b$) as the most reliable technique for NWM PBL height detection by NWP models (Zhang –et al., 2014). The bulk Richardson number is an approximation of the gradient Richardson number, which anticipates thermal convection via thermal energy, despite the resistance of turbulent kinetic energy referred to as wind shear:

$$R_b = \frac{\frac{g}{T_v}\Delta\theta_v \Delta Z}{(\Delta U)^2+(\Delta V)^2} \quad (1)$$

where g is the gravitational force , $T_v$ is the virtual temperature , $\Delta\theta_v$ is the difference in the virtual potential temperature along a vertical height of $\Delta z$ , $\Delta U$ and $\Delta V$ is the difference in the horizontal wind speed components. Essentially, the bulk Richardson number is a dimensionless ratio between the two main forces in the troposphere, namely, buoyancy and wind shear.

The bulk Richardson number formula for a certain height (Hanna R. Steven-,1969, Zhang et al., 2014) is given in the following manner:

$$R_b = \frac{\frac{g}{\theta_v}(\theta_{vz}-\theta_{v0})(Z-Z_0)}{U^2+V^2} \quad (21)$$

where g is the gravitational force, $\theta_{vz}$ is the virtual potential temperature at height Z, $\theta_{v0}$ is the virtual potential temperature at ground level ($Z_0$) ( hence equals the virtual temperature - $T_v$), U and ). U and V are the horizontal wind speed components at height Z.

The IFS model defines the PBL height as the lowest height level at which the bulk Richardson number$R_b$ (Eq. 21) reaches a critical threshold of 0.25 (ECMWF-IFS documentation – Cy43r3, Part IV: Physical Processes, July 2017). The PBL height is distinguished by scanning the bulk Richardson resultsvalues from the surface level upwards. WhenIf the PBL height is found between two levels of the model, it is determined by linear interpolation.

Radiosonde's profiles were analyzed in the same manner by a $R_b$ threshold of 0.25 to detect a specific height rather than a certain layer.

COSMO estimates the ~~bulk Richardson number~~$R_b$ based on the dynamic conditions of the first four levels (10, 34.2, 67.9, 112.3 m a.g.l.) signified by a threshold of 0.33 for stable conditions and 0.22 for unstable ones. If no level is found, then a missing value is assigned for the PBL height.

~~In this study, the hot and dry summer nights of the Israeli summer produce stable SBL described by values that are higher than the aforementioned thresholds. Such cases inhibit PBL detection by the bulk Richardson number method. Consequently, we focused on the daytime hours between 9-14 UTC when convective conditions prevail.~~

### 5.2 The parcel method

The PBL height is defined by the parcel method ~~(Holzworth 1964, Stull, 1988, Seidel et al., 2010)~~ as the height aloft at which the value of the virtual potential temperature reaches ~~the~~ that of the surface level~~.~~ (Holzworth 1964, Stull, 1988, Seidel et al., 2010). The calculation of the virtual potential temperature is as follows:

$$\theta_v = T_v \left(\frac{P_0}{P}\right)^{\frac{Rd}{Cp}} \quad (32)$$

where $P_0$ is the ground level atmospheric pressure, $P$ is the at atmospheric pressure at height Z, $R_d$ is the gas constant of dry air, $C_p$ is the heat capacity of dry air in a constant pressure ($\frac{R_d}{C_p}$ = 0.286).

The virtual temperature ($T_v$) is obtained by:

$$T_v = \frac{T}{1-\frac{e}{P}(1-\varepsilon)} \quad (43)$$

where T is the temperature at height Z, $e$ is the actual vapor pressure and $\varepsilon$ is the ratio of the gas constant of air and water vapor ($\varepsilon$=0.622). The actual vapor pressure ($e$~~, Eq. (5))~~) is derived by the relative humidity (RH) profile~~.~~ multiplied by the saturated vapor pressure ($e_s$). The saturated vapor pressure ~~($e_s$) is calculated by Eq. (6) based on~~was derived by the temperature profile.

~~$e = e_s \frac{RH}{100}$ (5)~~

~~$e_s = 610.78 \exp\left(\frac{T}{T+238.3} 17.2694\right)$ (6)~~

~~The IFS model creates profiles of specific humidity instead of RH, hence, we calculated the actual vapor pressure ($e$), given in Eq. (5), by the following equation:~~

~~$e = \frac{qP}{0.378q+\varepsilon}$ (7)~~

~~where q is the specific humidity, P is the pressure at the height Z, and $\varepsilon$ is the ratio of the gas constant of air and water vapor ($\varepsilon$=0.622).~~

In this method, the value of the virtual potential temperature at surface height is crucial. The first levels of IFS and COSMO are 10 m a.g.l and 20 m a.g.l, respectively. Thus, evaluations of the ambient temperature and the dew point temperature (or RH) for 2 m a.g.l are generated by the models based on the similarity theory.

### 5.3 The wavelet covariance transform method

~~In our study, ceilometer PBL height is detected by the backscatter profiles above the height of the overlap function (~ 100 m, see Sect. 2.1). When clouds are present (mainly summer shallow cumulous), the algorithm defines the top of the clouds, denoted as the height were the signal counts decrease to the amount retrieved by background values. The cloud top height is defined as the PBL height, signifying the height where the shallow convective cloud updrafts cease and the free atmosphere begins (Stull, 1988). If no clouds exist, the algorithm defines an upper limit as the lowest height among two categories: the point with the highest variance between consecutive steps (20 m resolution), or the first point with negative values corresponding to low signal-to-noise ratio. Finally, the~~The wavelet covariance transform (WCT) method is operated along the length of the backscatter profile ~~within the aforementioned height limits.~~

~~The WCT method~~ (Brooks Ian, 2003~~),~~). This method is based on the Haar step function (Baars et al., 2012~~, is~~) given in Eq. (~~8~~4) and Eq. (~~9~~5) as follows:

$$W_{f(a,b)} = \frac{1}{a}\int_{Zb}^{Zt} f(z)h\left(\frac{z-b}{a}\right)dz \quad (8)$$

where $W_{f(a,b)}$ is the local maximum ~~along~~of the backscatter profile ($f(z)$~~),~~) determined within the range of step (a~~) defined by~~). The length of the step is the number of height levels (n) multiplied by the ~~profiles~~profile height resolution (~~$a = n$~~ $\Delta z$~~). The profile's lower~~) from ground level (Zb) and ~~upper~~up (Zt~~) boundaries and the~~).

The Haar step function, given in Eq. (~~9~~(5), is equivalent to a derivative at height $z$, representing the value difference of each step ($a$) above and beneath a point of interest ($b$). Here, b is the measurement heights of the ceilometer along the profile (every 10 m starting from 10 m a.g.l) and step a was defined as 20 m (10 m above and beneath point b).

$$h\left(\frac{z-b}{a}\right) = \begin{Bmatrix} +1, & b - \frac{a}{2} \le z \le b, \\ -1, & b \le z \le b + \frac{a}{2} \\ 0, & elsewhere \end{Bmatrix} \quad (95)$$

~~The Haar function is equivalent to a derivative, representing the value difference of each step above and beneath the point of interest ($b$). On clear days, the highest derivative (local maximum) occurs at the transition zone between the CBL and the free atmosphere. When clouds do exist, the strongest gradients appear when light emitted by the ceilometer encounters the cloud aerosols, and the local maximum is indicated as the cloud base height. However, as previously mentioned, our algorithm denotes the PBL height as the top of the shallow cloud (Stull, 1988).~~

To evaluate the ceilometers' PBL heights (Eq. 4), the backscatter profiles are analyzed by the WCT method between two boundaries. The lower boundary (Zb) is the height above the perturbation of the overlap function (~ 100 m, see Sect. 4.1). The upper limit (Zt) is either the height point with the largest variance within a step or the first height point with negative values indicating a low signal-to-noise ratio. The lowest height among the two aforementioned options will define the upper limit.

When clouds exist (mainly shallow cumulus clouds), the algorithm defines the PBL height as the highest measurement point of the cloud above the cloud base height. This height indicates the entrainment zone rather than the actual cloud top.

## 6. Results

### 6.1 Comparison to in-situ radiosonde profiles

~~Statistical analysis of~~In order to evaluate the ~~Beit Dagan~~daytime PBL heights produced by the models and the ceilometers, the results were compared to the radiosonde's evaluations. Consequently, the investigation was held in Beit Dagan launch site at the time of the midday launch (11 UTC). For this comparison, the ceilometer's 15 s profiles were averaged as half-hour profiles between 10:30-11:00 UTC. COSMO's results referred to the profiles of 10:45 UTC, and IFS estimations were given at 11 UTC. The analysis was carried out for 33 summer days, 13 days from August 2015, and 20 days from Aug 2016. The PBL heights were produced by the same methods: the parcel method (denoted by subscript P) and the bulk Richardson method (denoted by subscript R). These methods require meteorological parameters such as temperature and pressure profiles generated by the models and the radiosonde. Ceilometers, on the other hand, produce only backscatter signals. Therefore, they were analyzed by the WCT method. The results were statistically analyzed by mean error (ME), root mean square error (RMSE), and correlation (R) ~~is~~ presented ~~(~~in Fig. 2~~,~~ and Table 3~~) at 11 UTC from radiosonde profiles, the Beit Dagan ceilometer, and the two models. The PBL heights were derived by the bulk Richardson method (denoted by subscript R) and the parcel method (denoted by subscript P). The analysis was carried out for 33 summer days (13 days from August 2015 and 20 from Aug 2016) available from all models and instruments. The PBL heights of the radiosonde obtained the same results by either method ($RS_P$, $RS_R$) and this was the base of comparison. The best~~.

Good agreement was found between the ceilometer and the radiosonde ~~results (ME=12, RMSE=97, and R=0.93). A large gap (800 m)~~(ME = 12 m, RMSE = 97 m, and R = 0.93), although they produced the PBL heights by different methods. Among the models and methods, $COSMO_R$ retrieved the best results of ME = -3 m, RMSE = 152 m and R = 0.83). IFS predominantly overestimated the PBL heights. The poorest results were generated by $IFS_R$ (ME = 274 m, RMSE = 432 m, R = 0.18).

An example of an analysis on a typical day is given in Fig. 3 for August 15, 2015. On this day, the PBL height at 11 UTC was estimated at 680 m a.s.l by the radiosonde. $COSMO_P$ accurately estimated the same height while $COSMO_R$ detected the height to be 100 m lower (580 m a.s.l). The ceilometer overestimated by 100 m (795 m a.s.l). IFS results were twice the value produced by the radiosonde ($IFS_R$=1,300 m a.s.l, $IFS_P$= 1,474 m a.s.l).

Among the 33 days tested, the largest gap was found between $IFS_R$ and ~~the radiosonde's PBL~~ $RS_R$ on August 17, 2016 ~~consisting of an uncommon multi-cloud layer. Consequently, the recorded~~(Fig. 2). The imprecision could be due to the fact that the Richardson method is based solely on dry thermodynamics for local turbulence (Von Engeln and Teixeira, 2013), while on August 17, 2016, the 11 UTC PBL height was determined through a multi-layer cloud ~~formation (Fig.3). Nevertheless, COSMO results based on the parcel method ($COSMO_P$) managed to retain the radiosonde's PBL height despite cloud formation. Overall, the Beit Dagan ceilometer's estimations show the best results. Therefore, the PBL measured by five ceilometers (including Beit Dagan) will be used as a reference for the spatial analysis where radiosonde measurements are (~~not ~~performed.~~shown).

### 6.2 Spatial analysis by ceilometers

~~In~~After the ~~next stage,~~ good results generated by the WCT method imposed on the ceilometer's profiles, ceilometers were applied as PBL height detectors in sited where no other atmospheric measurements operated. The same analysis process was carried out ~~at 11 UTC; this time, however, instead of focusing on only one location, it was performed on~~but for five ceilometer sites (Ramat David, Tel Aviv, Beit Dagan, Weizmann, and Jerusalem~~). Yet, in order to include the Beit Dagan single radiosonde launching in the PBL height measurements under uniform meteorological conditions, we were limited to 13 dates. When we evaluated~~), representing diverse terrain on 13 specific days available from all instruments and models. This time the models' ~~grid points corresponding~~results were compared to the ceilometers' ~~sites, we discovered both~~measurements in each site. Both models defined the Tel Aviv ~~within~~site by a grid point ~~that was~~ mostly over the Mediterranean Sea. Therefore, we shifted the Tel Aviv ~~site~~coordinates to an adjacent grid point that was mostly land, representing ~~the~~ Tel Aviv ~~site in~~by the same height and distance from the shoreline ~~within a grid point that was mostly land~~.

~~Exploration of the spatial evolution of the PBL height was implemented on 13 specific days retaining data from all instruments and models. Figure 4 presents the PBL height over five ceilometer sites representing diverse terrain. The~~A comparison to ~~the~~ radiosonde's ~~PBL heights revealed a~~results was available only in Beit Dagan. Figure 4b reveals a good agreement between the radiosonde and the ceilometer's evaluations in Beit Dagan, although the different methods imposed on each instrument. A significant case on August 10, 2015, where ~~all models overestimated the PBL height. Inspection models and radiosonde virtual potential temperature profiles for August 10, 2015 (Fig. 5) showed that~~ an ~~additional~~atmospheric layer ~~aloft affected~~

above the PBL height denoted by the radiosonde and the ~~overestimation of the models leading~~ceilometer (not shown) led to the ~~discrepancy~~models' discrepancies.

~~Inspection of the IFS results by both methods ($IFS_R$, $IFS_P$) revealed the model's limited capacity to precisely represent the PBL heights of specific sites even over flat terrain. This is expressed by overestimations in Tel Aviv (5 m a.s.l) and Beit Dagan (33 m a.s.l) given as RMSEs of 276-568 (Table 4). On the one hand, lower RMSEs (173-278, Table 4) were calculated in Weizmann (60 m a.s.l) and Ramat David (50 m a.s.l) sites.~~

~~Largely, COSMO PBL height based on the bulk Richardson method ($COSMO_R$) achieved the best statistical results (Tables 4-5) regarding flat and complex terrain altogether.~~

By and large, $COSMO_R$ achieved the best statistical results (Tables 4-5) regarding flat and complex terrain, of RMSE from 175 m in Weizmann (60 m a.s.l, and 11.5 km east from the shoreline) up to 251 m in Jerusalem (830 m a.s.l and 53 km east from the shoreline), and ME between 19 m in Tel Aviv (5 m a.s.l, and 50 m from shoreline), and -26 m in Ramat David (50 m a.s.l, and 24 km east from the shoreline). $IFS_P$ produced high RMSE results starting at 180 m in Ramat David rising up to 569 m in Beit Dagan, and ME up to 497 m in Beit Dagan. These results emphasize the advantage of high-resolution regional models such as COSMO (~2.5 km resolution) over the IFS global model (resolution of ~13 km in 2015 and ~10 km in 2016) over a diverse area.

### 6.3 COSMO PBL height correction

Finally, ~~we analyzed~~ the spatial ~~evolution~~daytime summer PBL heights were investigated. Following the conclusions of ~~the PBL height over Israel based on~~previous stages, $COSMO_R$. ~~The COSMO~~ was chosen as the model ~~at 2.5 km resolution~~and method that achieved the best results. Average hourly values were ~~compared to the PBL heights discerned by eight ceilometer sites (Fig. 1, Table 1) for the daytime hours~~derived between ~~9 -~~ 09-14 UTC (corresponding to 11 -16 LST~~). Correction of~~) and compared to the results from eight ceilometer sites (Fig. 1, Table 1). The comparison was accomplished by all dates available for each ceilometer site on August 2015: Jerusalem - 21 days, Nevatim - 13 days, Hazerim - 20 days, Ramat David - 26 days, Weizmann - 25 days, Beit Dagan - 13 days, Hadera - 16 days, Tel Aviv - 25 days.

In order to validate and correct $COSMO_R$ results ~~was made by means of a~~ by the ceilometers' measurements, a correction tool based on a regression function was implemented ~~separately~~ for each hour~~,~~ (09-14 UTC), for all ceilometers' sites simultaneously~~. The regression~~ by the following formula ~~is as follows~~:

$$ME_{st} = \alpha G + \beta D + \gamma \quad (\text{~~10~~6})$$

where $ME_{st}$ is the dependent variable representing the PBL height mean error for each ceilometer station (st) compared to the results obtained by the $COSMO_R$. The independent predictor variables are the ground altitude of the ceilometer's site (G) and its distance from the shoreline (D). The correction factors α, β, and γ are implemented on the $COSMO_R$ PBL height results.

~~We must note that here, the mean error PBL height was based on all available dates for each site on August 2015, as detailed in the following figures. Figure 6 demonstrates the correction process for 14 UTC with a maximum correction of ~300 m over a complex terrain surrounding Jerusalem (830 m a.s.l) and Nevatim (400 m a.s.l). A summary of the correction results appears in Fig. 7. Apparently, this correction reduced the COSMO diurnal PBL height difference. As expected (see Sect. 2), at 9 UTC the PBL height is the highest over Tel Aviv and the lowest over Jerusalem. At 11 UTC, however, an opposite process occurs as the PBL height descends near the shore and ascends over mountainous Jerusalem. Finally, at 14 UTC, as the solar insolation decreases, Tel Aviv PBL height is ~200 m lower than evaluated for midday (9 UTC), slowly descending over Jerusalem as well.~~

~~7.~~$COSMO_R$ mean PBL heights cross-section from Tel Aviv (34.8° lat) to Jerusalem (35.2° lat) is presented in Fig. 5. Before the correction (Fig. 5a), $COSMO_R$ approximated Tel Aviv PBL heights descend gradually from 750 at 09 UTC (11 LST) to 600 m a.s.l at 14 UTC (16 LST). Apparently, the correction tool reduced the height difference to ~700 m a.s.l with the exception of ~750 m a.s.l at 09 UTC (Fig. 5b). These results correspond to Uzan et al, (2012) showing Tel Aviv site is practically on the shoreline, therefore as the sea breeze enters Tel Aviv (~ 08 UTC), it surmounts the convective thermals preventing from the mixed layer to inflate.

In Jerusalem, the summer PBL height inflates according to the insolation intensity, as the main source of the buoyancy force. Therefore, the maximum daytime PBL heights are measured at midday. In the afternoon, when the sea breeze reaches eastern Israel, the height decreases. $COSMO_R$ results before and after the correction showed the highest value at 11 UTC (13 LST), corresponding to maximum insolation at midday. The lowest value was corrected from 09

UTC (11 LST) to 14 UTC (16 LST) as insolation decreases and the cool and humid air of sea breeze front demolishes the thermals and the PBL height subsides.

Between the shoreline of Tel Aviv and the eastern mountains of Jerusalem, the overall range of PBL height values was reduced. For example, in 35° lat (between Weizmann - 60 m a.s.l and Jerusalem - 830 m a.s.l), the PBL heights of 09-14 UTC varied from 750 to 1500 m a.s.l. After the correction, the height values ranged from 1000 to 1400 m a.s.l, generating higher PBL heights for the daytime hours. Fig. 6 demonstrated the correction tool at 14 UTC disclosing a correction of ~ 300 m (Fig. 6b) over the complex terrain of Jerusalem (830 m a.s.l) and Nevatim (400 m a.s.l).

## 7. Summary and Conclusions

Earlier studies have successfully employed ceilometers for PBL height detection, typically under dry conditions. However, these studies employed weather models primarily as a validation tool rather than investigating the models' predictive capabilities. Here, we tested the ~~accuracy~~ability of ceilometers to serve as a correction tool for PBL height estimations derived from two operational models~~,~~: the IFS global model ~~(~ 9 and ~16 km resolution),~~ and the ~~meso-scale~~mesoscale COSMO regional model ~~(~2.5 km resolution). ~~. The ~~models calculate~~study focused on the ~~PBL height by the bulk Richardson method. Therefore, the PBL height estimations were relevant to~~ daytime ~~convection, which focused upon 11 UTC in our study. The radiosonde and models' results were generated by the bulk Richardson method and the parcel method as well. The results were compared to the ceilometers'~~summer PBL heights ~~in August 2015 and 2016 detected by the WCT method~~.

~~We found the best correlation (0.91) and lowest RMSE (109 m) between the radiosonde's heights and the adjacent Beit Dagan ceilometer. Comparison of the~~ Firstly, we compared the models' ~~PBL heights to the ceilometers' heights in four additional sites without radiosonde~~ and the ceilometer's evaluations to actual measurements~~, it was found that COSMO~~ from an adjacent radiosonde in the Beit Dagan launch site. Results for 11 UTC on 33 August days revealed the promising ability of the WCT method to detect the PBL heights generated by the radiosonde by the bulk Richardson method and by the parcel method (RMSE= 97 m).

In the next stage, the investigation expanded spatially to four other diverse measuring sites, from the shoreline of Tel Aviv (5 m a.s.l) to the mountainous Jerusalem (830 m a.s.l). The same

methods were applied for 13 summer days, except this time, the models' values were compared to the ceilometers' measurements in each site. The results disclosed the COSMO model based on the bulk Richardson method ($COSMO_R$) achieved the ~~most in~~ best results for both flat (Tel Aviv: RMSE=203 m, ME=19 m) and ~~elevated~~complex terrain~~. Apparently, IFS overestimated the evolution of the PBL height as it progressed inland to the elevated Jerusalem site (830 m a.s.l~~ (Jerusalem: RMSE = 251m, ME = -6 m).

~~The combination of ceilometers and a high resolution COSMO model enabled us to generate, for the first time, a corrected spatial evolution of the daytime PBL (9-14 UTC) height over Israel.~~

Finally, the temporal and spatial evolution of the summer daytime (11-16 LST) PBL heights were examined. The heights were derived by $COSMO_R$ and compared to ceilometers measurements distributed in eight sites across Israel, providing a heterogeneous research area in comparatively short distances. A correction tool was established based on a regression function comprised of the topography of the ceilometer's site (G) and its distance from the shoreline (D) serving as the independent predictor variables. The results revealed corrections up to ~ 300 m difference which improved the description of the diurnal PBL heights.

Despite the limited database, our results offer a preview of the great potential of ceilometers as a validation and a correction tool to discern PBL ~~height~~heights derived from weather models. Future research should, therefore, include a larger dataset to evaluate whether these results are retained in the long term and to define a systematic validation process.

## Data availability

Weather reports- Israeli Meteorological Service weather reports (in Hebrew): http://www.ims.gov.il/IMS/CLIMATE/ClimateSummary.

Radiosonde profiles – Israeli Meteorological Service provided by request.

Ceilometer profiles - the data is owned by governmental offices~~. The~~, data is ~~not online and~~ provided by request.

## Author contribution

Leenes Uzan carried out the research and prepared the manuscript under the careful guidance of Pinhas Alpert and Smadar Egert alongside a fruitful collaboration with Yoav Levi, Pavel Khain and Elyakom Vladislavsky. The authors declare that they have no conflict of interest.

~~**Acknowledgements**~~

**Acknowledgments**

We wish to thank the Israeli Meteorological Service, the Israeli Air Force, the Association of Towns for Environmental Protection (Sharon-Carmel), and Rafat Qubaj from the Department of Earth and Planetary Sciences at the Weizmann Institute of Science, for their ceilometer data. We are indebted to Hadas Marcus for her editing assistance.

## References


Alpert P., and Ziv B.: The Sharav cyclone observations and some theoretical considerations, J. Geophys. Res., 94, 18495–18514, 1989.

Alpert P., Herman J., Kaufman Y. J., and Carmona I.: Response of the climatic temperature to dust forcing, inferred from TOMS Aerosol Index and the NASA assimilation model. J. Atmos. Res., 53, 3-14, 2000.

Alpert, P., Krichak, S. O., Tsidulko, M., Shafir, H., and Joseph, J. H.: A Dust Prediction System with TOMS Initialization, Mon. Weather Rev., 130, 2335–2345, 2002.

Alpert P., and Rabinovich-Hadar M.: Pre- and post-frontal lines - A meso gamma scale analysis over south Israel, J. Atmos. Sci., 60, 2994-3008, 2003.

Alpert, P., Osetinsky, I., Ziv, B., Shafir H.: Semi-objective classification for daily synoptic systems: Application to the eastern Mediterranean climate change. Int. J. of Climatol., 24, 1001-1011, 2004.

Baars, H., Ansmann, A., Engelmann, R., and Althausen, D.: Continuous monitoring of the boundary layer top with lidar, Atmos. Chem. Phys., 8, 7281–7296, https:// doi:10.5194/acp-8-7281-2008, 2008.

Baldauf, M., A. Seifert, J. Förstner, D. Majewski, M. Raschendorfer, and T. Reinhardt: Operational Convective-Scale Numerical Weather Prediction with the COSMO Model: Description and Sensitivities. Mon. Wea. Rev., 139, 3887–3905, https://doi.org/10.1175/MWR-D-10-05013.1, 2001.

Bechtold, P.: Convection parametrization. ECMWF Seminar proceedings on "The parametrization of subgrid physical processes", 63-85, 2008.

Brooks, I.: Finding Boundary Layer Top: Application of a wavelet covariance transform to lidar backscatter profiles, J. Atmos. Ocean. Tech., 20, 1092–1105, 2003.

Cerenzia I., Challenges and critical aspects in stable boundary layer representation in numerical weather prediction modeling: diagnostic analyses and proposals for improvement, Ph.D. thesis, University of Bologna, 2017.

Collaud Coen, M., Praz, C., Haefele, A., Ruffieux, D., Kaufmann, P., and Calpini, B.: Determination and climatology of the planetary boundary layer height above the Swiss plateau

by in situ and remote sensing measurements as well as by the COSMO-2 model, Atmos. Chem. Phys., 14, 13205-13221, https://doi.org/10.5194/acp-14-13205-2014, 2014.

Dayan, U., Shenhav, R., Graber, M.: The Spatial and temporal behavior of the mixed layer in Israel, J Appl Meteorol, 27, 1382- 1394, 1988.

Dayan, U., Rodnizki, J.: The temporal behavior of the atmospheric boundary layer in Israel. J Appl Meteorol, 38, 830-836, 1999.

Dayan, U., Lifshitz-Goldreich B., and Pick, K.: Spatial and structural variation of the atmospheric boundary layer during summer in Israel-Profiler and rawinsonde measurements. J. Appl. Meteor., 41, 447-457,2002.

Doms, G., J. Förstner, E. Heise, H.-J. Herzog, D. Mironov, M. Raschendorfer, T. Reinhardt, B. Ritter, R. Schrodin, J.-P. Schulz, and G. Vogel: A description of the nonhydrostatic regional COSMO model. Part II: Physical parameterization. Deutscher Wetterdienst, Ofenbach, 154 pp, 2011.

Eresmaa, N., Karppinen, A., Joffre, S. M., Räsänen, J., and Talvitie, H.: Mixing height determination by ceilometer, Atmos. Chem. Phys., 6, 1485-1493, https://doi.org/10.5194/acp-6-1485-2006, 2006.

Feliks, Y.: A numerical model for estimation of the diurnal fluctuation of the inversion height due to a sea breeze, Bound. Layer Meteor., 62, 151-161. 1993.

Feliks, Y: An analytical model of the diurnal oscillation of the inversion base due to sea breeze, J. Atmos. Sci., 51, 991-998,1994.

Feliks, Y: Nonlinear dynamics and chaos in the sea and land breeze, J. Atmos. Sci., 61, 2169-2187, 2004.

Gierens, R.T., Henriksson, S., Josipovic, M., Vakkari, V., Van Zyl, P.G., Beukes J.P., Wood, C.R., O'Connor, E.J.: Observing continental boundary layer structure and evolution over the South African savannah using a ceilometer, Theor. Appl. Climatoi., 136, 333-346, https://doi.org/10.1007/s00704-018-2484-7, 2018.

Haeffelin, M. and Angelini, F.: Evaluation of mixing height retrievals from automatic profiling lidars and ceilometers in view of future integrated networks in Europe, Bound. Lay. Meteorol., 143, 49–75, 2012.

Hanna, S. R.: The thickness of the planetary boundary layer, Atmos. Environ., 3, 519–536, 1969.

Hashmonay, R., Cohen, A., and Dayan, U.: Lidar observations of the atmospheric boundary layer in Jerusalem, J. Appl. Meteorol, 30, 1228-1236, 1991.

Holzworth, C. G.: Estimates of mean maximum mixing depths in the contiguous United States, Mon. Weather Rev., 92, 235–242, 1964.

Ketterer, C., Zieger, P., Bukowiecki, N.: Bound. Lay. Meteo., 151, 317-334, https://doi.org/10.1007/s10546-013-9897-8, 2014.

Koehler, M., Ahlgrimm, M. and Beljaars, A.: Unified treatment of dry convective and stratocumulus-topped boundary layers in the ECMWF model, Q. J. R. Meteorol. Soc., 137, 43-57, 2011.

Kotthaus, S. and Grimmond, C.S.B.: Atmospheric boundary-layer characteristics from ceilometer measurements. Part 1: a new method to track mixed layer height and classify clouds, Q J R Meteorol. Soc.,144 (714), 1525–1538, https://doi.org/10.1002/qj.3299, 2018.

~~Kuhn, P., Wirtz, M., Killius, N., Wilbert, S., Bosch, J.L., Hanrieder, N., Nouri, B., Kleissle, J., Ramirez, L., Schroedter-Homscheidt, M., Heinemann, D., Kazantzidis, A., Blanc, P. and Pitz-Paal, R.: Benchmarking three low-cost, low-maintenance cloud height measurement systems and ECMWF cloud heights, Sol. Energy, 168, 140-152, https://doi.org/10.1016/j.solener.2018.02.050, 2018.~~

Levi Y., Shilo E., and Setter I.: Climatology of a summer coastal boundary layer with 1290-MHz wind profiler radar and a WRF simulation, J. Appl. Meteorol. Climatol., 50, 1815-1826, https://doi.org/10.1175/2011JAMC2598.1, 2011.

Lieman, R. and Alpert, P.: Investigation of the planetary boundary ~~Layer~~layer height variations over complex terrain, Bound. Lay. Meteorol., 62, 129-142, 1993.

Mamouri, R.E., Ansmann, A., Nisantzi, A., Solomos, S., Kallos, G~~.~~., and Hadjimitsis, D.G.: Extreme dust storm over the Eastern Mediterranean in September 2015: satellite, lidar, and surface observations in the Cyprus region, Atmos. Chem. Phys., 16(21), 13711-13724, 2016.

Neumann J.: Diurnal variations of the subsidence inversion and associated radio wave propagation phenomena over the coastal area of Israel. Isr. Met. Serv, 1952.

Neumann J.: On the rotation rate of the direction of sea and land breezes. J. Atmos. Sci., 34, 1913-1917, 1977.

~~Szintai B., and Kaufmann P.: TKE as a measure of turbulence, Calibration of COSMO model, COSMO Newsletter No. 8, 2008.~~

Seidel, D. J., Ao, C. O., and Li, K.: Estimating climatological planetary boundary layer heights from radiosonde observations: Comparison of methods and uncertainty analysis, J. Geophys. Res., 115, D16113, doi:10.1029/2009JD013680, 2010.

Steppeler J., Doms G., Schattler U., Bitzer HW, Gassmann A., Damrath U., Gregoric G.: Meso gamma scale forecasts by nonhydrostatic model LM. Meteorological Atmospheric Physics, 82, 75–96, 2003.

Stull R.B.: An introduction to boundary layer meteorology, Kluwer Academic ~~publishers~~Publishers, the Netherlands, 666 p., 1988.

Tiedtke, M., 1989: A Comprehensive Mass Flux Scheme for Cumulus Parameterization in Large-Scale Models. Mon. Wea. Rev., 117, 1779–1800, https://doi.org/10.1175/1520-0493, 1989~~.~~.

Uzan, L. and Alpert, P.: The coastal boundary layer and air pollution - a high temporal resolution analysis in the East Mediterranean Coast, The Open Atmospheric Science Journal, 6, 9–18, 2012.

Uzan, L., Egert, S., and Alpert, P.: Ceilometer evaluation of the eastern Mediterranean summer boundary layer height – first study of two Israeli sites, Atmos. Meas. Tech., 9, 4387–4398, https://doi.org/10.5194/amt-9-4387-2016, 2016.

Von Engeln A., and Teixeira J.: A planetary boundary layer height climatology derived from ECMWF reanalysis data. J. Climate., 126, 6575-6590, https://doi.org/10.1175/JCLI-D-12-00385, 2013.

Wiegner M., Madonna F., Binietoglou I., Forkel R., Gasteiger J., Geiß A., Pappalardo G., Schäfer K., and Thomas W.: What is the benefit of ceilometers for aerosol remote sensing? An answer from EARLINET, Atmos. Meas. Tech., 7, 1979–1997, https://doi.org/10.5194/amt-7-1979-2014, 2014.

Wiegner, M. and Gasteiger, J.: Correction of water vapor absorption for aerosol remote sensing with ceilometers, Atmos. Meas. Tech., 8, 3971–3984, https://doi.org/10.5194/amt-8-3971-2015, 2015.

Yuval, Dayan, U., Levy, I., & Broday, D. M: On the association between characteristics of the atmospheric boundary layer and air pollution concentrations, Atmospheric Research, doi.org/10.1016/j.atmosers.2019.104675, 2019.

Zhang, Y., Gao, Z., Li, D., Li, Y., Zhang, N., Zhao, X., and Chen, J.: On the computation of planetary boundary-layer height using the bulk Richardson number method, Geosci. Model Dev., 7, 2599-2611, https://doi.org/10.5194/gmd-7-2599-2014, 2014.

Table 1. ~~Ceilometers parameters~~Location of measurements sites and ceilometer types

| Location | Site | Long/Lat | Distance from shoreline (km) | Height (m a.s.l) | Ceilometer type (resolution, height limit[a]) |
|---|---|---|---|---|---|
| Ramat David (RD) | North | 32.7 °/35.2 ° | 24 | 50 | CL31 (10 m,16 s, up to 7.7 km) |
| Hadera (HD) | Shoreline | 32.5 °/34.9 ° | 3.5 | 10 | CL31 (10 m,16 s, up to 7.7 km) |
| Tel Aviv (TLV) | Shoreline | 32.1 °/34.8 ° | 0.05 | 5 | CL31 (10 m,16 s, up to 7.7 km) |
| Beit Dagan (BD)[b] | Inland | 32.0 °/34.8 ° | 7.5 | 33 | CL31 (10 m,15 s, up to 7.7 km) |
| Weizmann (WZ) | Inland | 31.9 °/34.8 ° | 11.5 | 60 | CL51 (10 m,16 s, up to 15.4 km) |
| Jerusalem (JR) | Mountain | 31.8 °/35.2 ° | 53 | 830 | CL31 (10 m,16 s, up to 7.7 km) |
| Nevatim (NV) | South | 31.2 °/34.9 ° | 44 | 400 | CL31 (10 m,16 s, up to 7.7 km) |
| Hazerim (HZ) | South | 31.2 °/34.7 ° | 70 | 200 | CL31 (10 m,16 s, up to 7.7 km) |

[a]The height limit depends on sky conditions and decreases as the atmospheric optical density (AOD) increases. Data acquisition was limited to 4.5 km by the ceilometers' software (BLview), except ~~for~~ in Beit Dagan.
[b]The location of ceilometer Beit Dagan and the radiosonde launch site.

Table 2. ~~Characteristics~~Parameters of the NWP models

| Model | Operation center | Resolution (deg) | Type | Convection parametrization |
|---|---|---|---|---|
| COSMO | IMS | 0.025 | Regional, boundary conditions from IFS | Mass flux Tiedtke shallow convection |
| IFS | ECMWF | 0.1 in 2015<br>0.125 in 2016 | Global | Mass flux Tiedke-Bechtold |

765 Table 3. Statistical analysis of the Beit Dagan PBL heights on 33 summer days (13 days ~~in~~on August 2015 and 20 days ~~in~~on August~~,~~ 2016) from IFS and COSMO models by the bulk Richardson method ($IFS_R$, $COSMO_R$), the parcel method ($IFS_P$, $COSMO_P$) and the WCT method for the adjacent ceilometer. The PBL heights were compared to those derived from Beit Dagan radiosonde by either the parcel or bulk Richardson methods (same results, see Fig 770 2).

| PBL detection | $IFS_R$ | $IFS_P$ | $COSMO_R$ | $COSMO_P$ | Ceilometer |
|---|---|---|---|---|---|
| Mean Error (m) | 274 | ~~249~~271 | -3 | -~~17~~106 | 12 |
| RMSE (m) | 432 | ~~409~~411 | 152 | ~~179~~176 | 97 |
| R | 0.18 | 0.~~18~~21 | 0.83 | 0.~~73~~83 | 0.93 |
| Mean PBL (m a.s.l) | 1250 | ~~1225~~1247 | 973 | ~~959~~869 | 989 |
| Std PBL (m) | 274 | ~~256~~ 245 | 273 | ~~229~~222 | 259 |

Table 4. Root mean square errors of PBL heights from five sites on 13 summer days (Fig. 4), derived by IFS and COSMO models by the bulk Richardson method ($IFS_R$, $COSMO_R$) and the 775 parcel method ($IFS_P$, $COSMO_P$). The PBL heights were compared to the heights measured by the Beit Dagan ceilometer.

| Site | $IFS_R$ | $IFS_P$ | $COSMO_R$ | $COSMO_P$ |
|---|---|---|---|---|
| Ramat David | 173 m | ~~191~~180 m | 247 m | ~~241~~232 m |
| Tel Aviv | 276 m | ~~465~~498 m | 203 m | ~~183~~182 m |
| Beit Dagan | 405 m | 569 m | 235 m | ~~234~~171 m |
| Weizmann | 214 m | ~~274~~339 m | 175 m | ~~145~~209 m |
| Jerusalem | 351 m | ~~368~~285 m | 251 m | ~~273~~179 m |

780 Table 5. Same as in Table 3 but for mean errors.

| Site | $IFS_R$ | $IFS_P$ | $COSMO_R$ | $COSMO_P$ |
|---|---|---|---|---|
| Ramat David | -31 m | ~~300~~ m | -26 m | ~~0~~-12 m |
| Tel Aviv | 234 m | ~~376~~422 m | 19 m | -35 m |
| Beit Dagan | 332 m | 497 m | 12 m | -~~9~~55 m |
| Weizmann | 114 m | ~~218~~280 m | 16 m | -42 m |
| Jerusalem | 298 m | ~~327~~243 m | -6 m | ~~29~~-1 m |

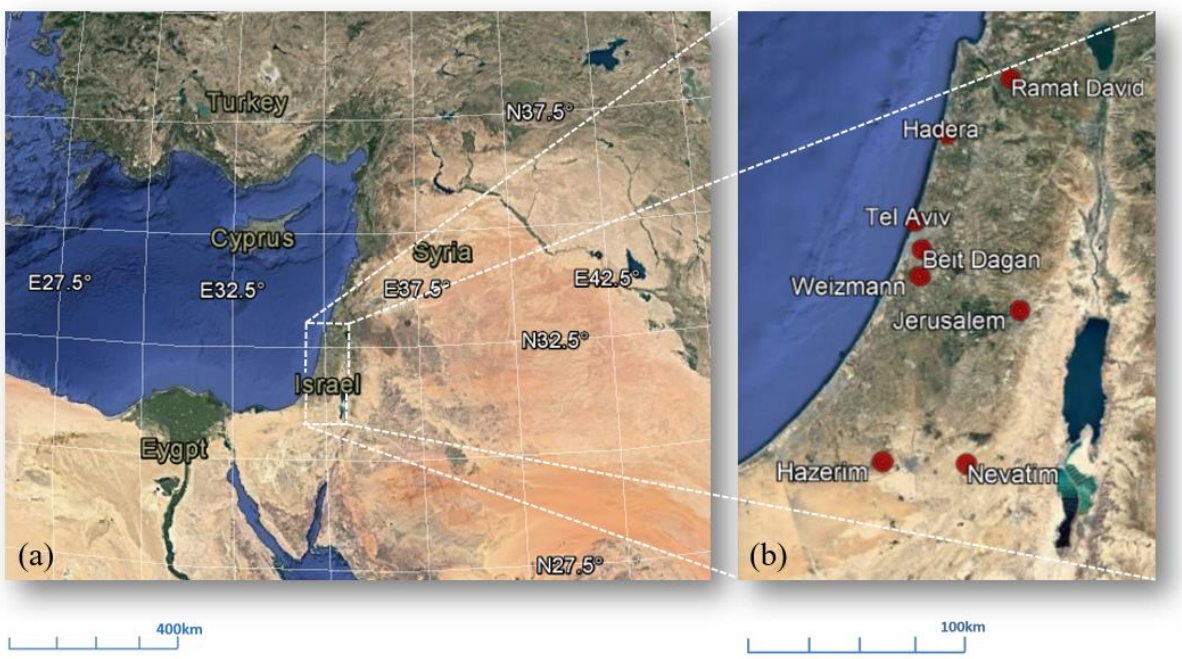


785 Fig. 1 Maps of (a) the East Mediterranean and (b) the research area including indications of the ceilometers sites (red circles). The Radiosonde launch site is situated in Beit Dagan, adjacent to the ceilometer. Adapted from © Google Maps 2019.

790

795

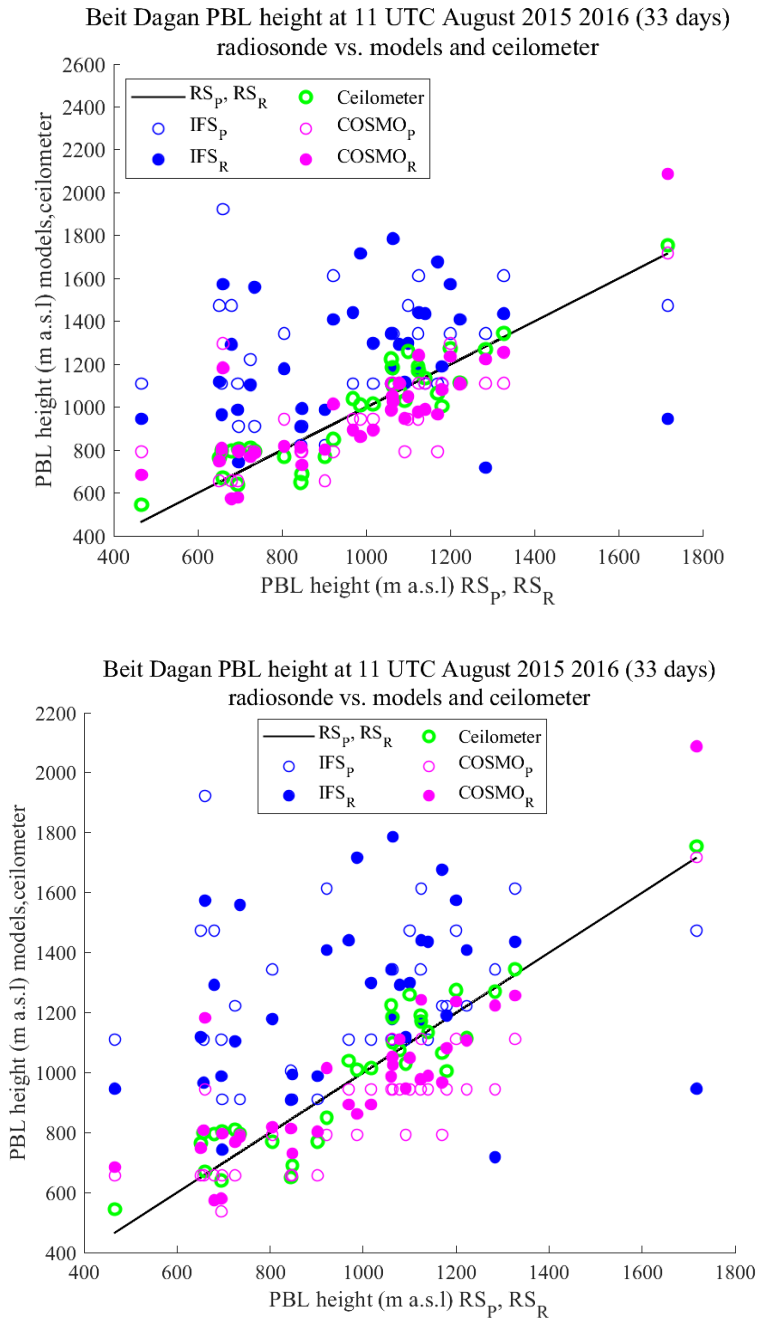


Fig 2. PBL heights over Beit Dagan site on 33 summer days (13 days on August 2015 and 20 days on August 2016), generated by the bulk Richardson method for IFS model ($IFS_R$, blue solid circles), COSMO model ($COSMO_R$, pink solid circles), and Beit Dagan radiosonde profiles ($RS_R$, black line). PBL heights generated by the parcel method for the IFS model ($IFS_P$, open blue circles), COSMO model ($COSMO_P$, open pink circles), and Beit Dagan radiosonde profiles ($RS_P$, same black line as $RS_R$, the results are identical). PBL heights derived from the Beit Dagan ceilometer were produced by the WCT method (green circles). Extreme Results (up to ~2, 00 m a.s.l) for August 17, 2016, are shown on the right-hand side.

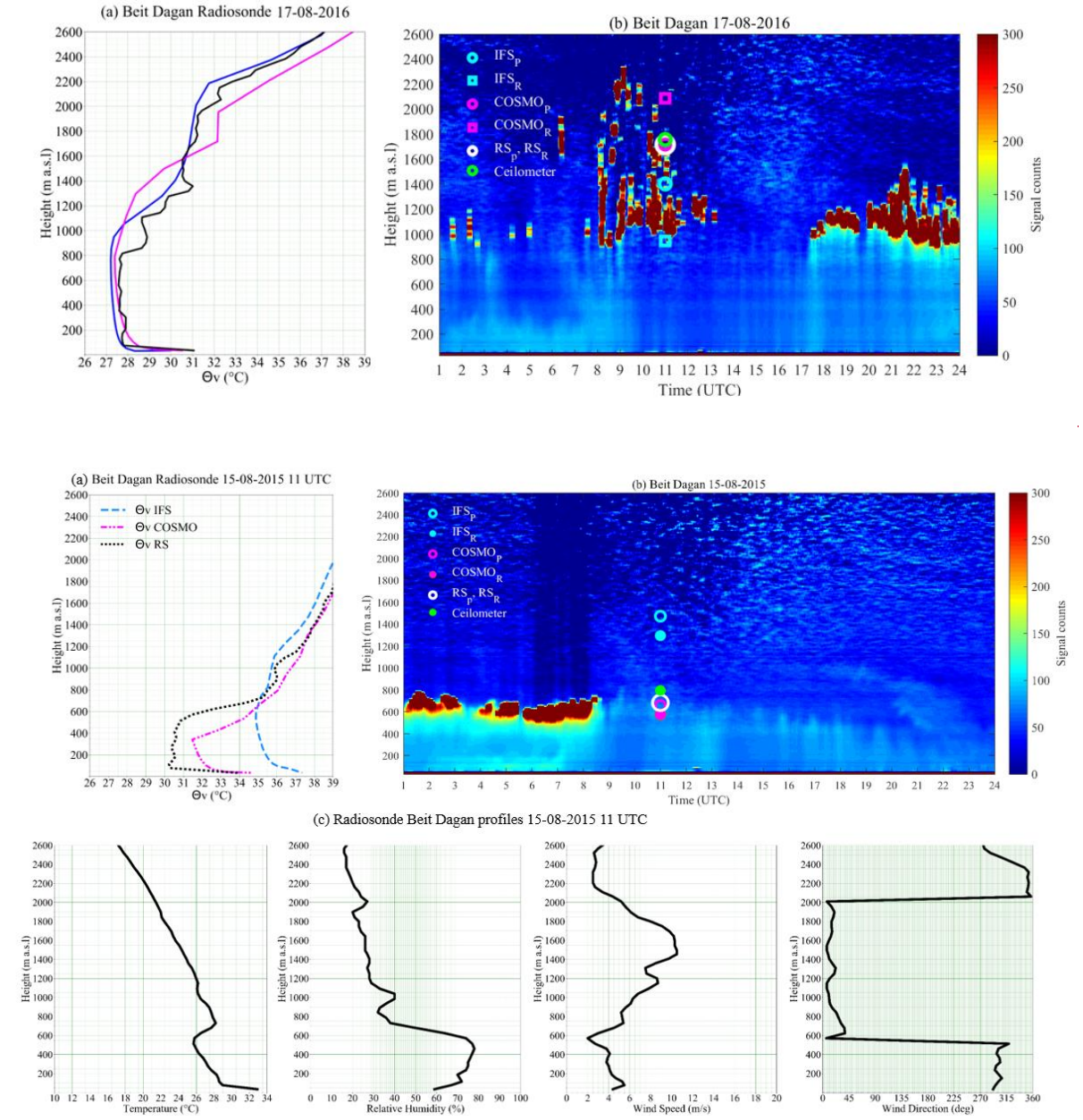


Fig.3 Meteorological measurements from Beit Dagan site on August 15, 2015: Virtual potential temperature profiles ~~(a)~~at 11 UTC generated from ~~Beit Dagan~~ radiosonde ~~(black lines),~~measurements, IFS ~~model (blue lines)~~ and COSMO ~~model (pink lines) and, (b)~~models (a), ceilometer signal counts plot ~~on August 17, 2016~~ including indications of the PBL heights at 11 UTC from the models ($IFS_R$, $IFS_P$, $COSMO_R$, $COSMO_P$), radiosonde ($RS_R$, $RS_P$) and ceilometer~~.~~ (b). The bottom panel presents radiosonde profiles of temperature, RH, wind speed and wind direction at 11 UTC (c).

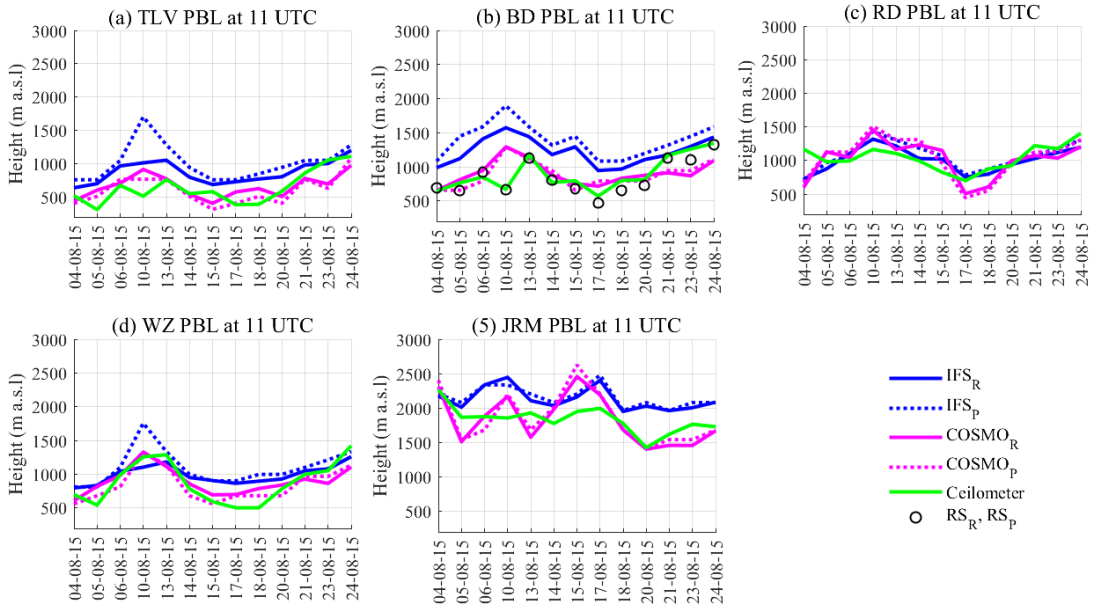


Fig. 4 PBL heights on 13 August days in 2015 from five ceilometer sites: (a) Tel Aviv (TLV), (b) Beit Dagan (BD), (c) Ramat David (RD), (d) Weizmann (WZ), and (e) Jerusalem (JRM). PBL heights were generated by the bulk Richardson method for the IFS model ($IFS_R$, blue solid line) and the COSMO model ($COSMO_R$, pink solid line). PBL heights generated by the parcel method for the IFS model ($IFS_P$, blue dashed line) and the COSMO model ($COSMO_P$, pink dashed line). Beit Dagan radiosonde profiles ($RS_R$, $RS_P$, black circles). PBL heights derived from the ~~Beit Dagan ceilometer~~ceilometers (green line) were produced by the WCT method.

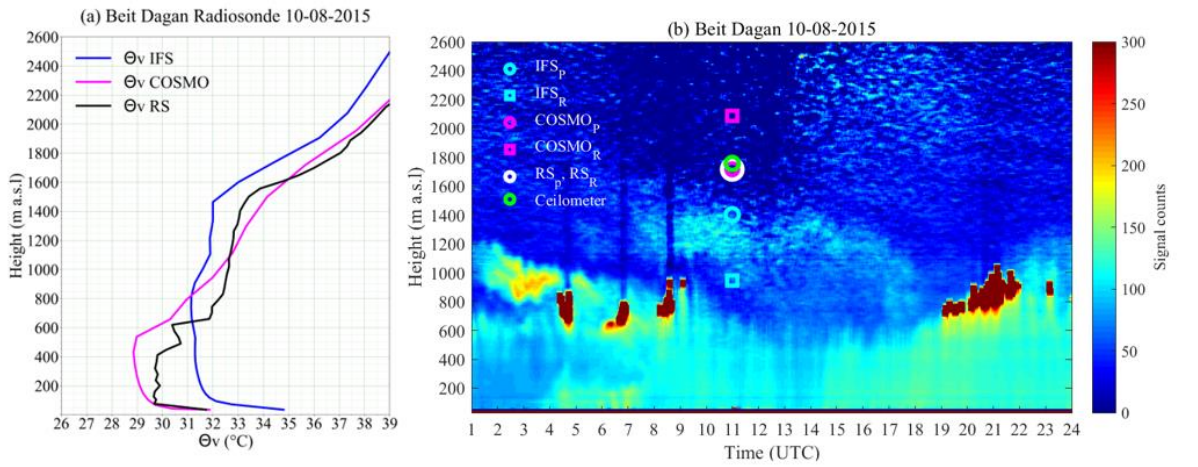


~~Fig.5 Virtual potential temperature profiles (a) from Beit Dagan radiosonde (black lines), IFS model (blue lines) and COSMO model (pink lines) and, (b) ceilometer signal counts plot on August 10, 2015 including indications of the PBL heights from the models ($IFS_R$, $IFS_P$, $COSMO_R$, $COSMO_P$), radiosonde ($RS_R$, $RS_P$) and ceilometer.~~

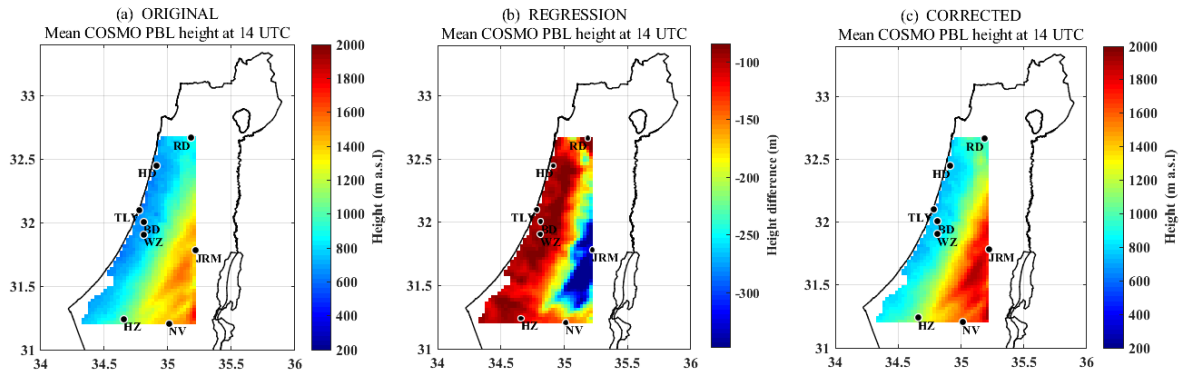


845

~~Fig. 6 Three dimensional maps of $COSMO_R$ mean PBL heights over Israel at 14 UTC before (a) and after (c) correction. The regression (b) given in Eq. (10) depicts the height difference between $COSMO_R$ and the ceilometers.~~

850

~~The analysis was performed on the number of available days for each site on August 2015 as follows: Jerusalem - 21 days, Nevatim - 13 days, Hazerim - 20 days, Ramat David - 26 days, Weizmann - 25 days, Beit Dagan - 13 days, Hadera - 16 days, Tel Aviv - 25 days.~~

855

860

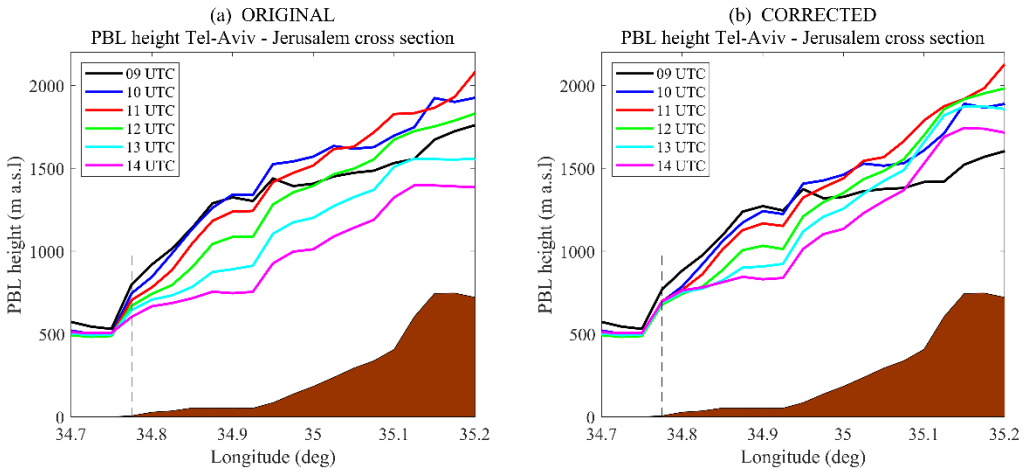


865 Fig. ~~7~~5 $COSMO_R$ mean PBL height cross-~~-~~section from Tel Aviv to Jerusalem before (a) and after (b) correction between 9-14 UTC. The analysis was performed on the number of available days for each site on August 2015 as follows: Jerusalem - 21 days, Nevatim - 13 days, Hazerim - 20 days, Ramat David - 26 days, Weizmann - 25 days, Beit Dagan - 13 days, Hadera - 16 days, Tel Aviv - 25 days. ~~The~~Indications of the seashore (dashed line) and the topography
870 (brown area) are ~~also shown~~given.

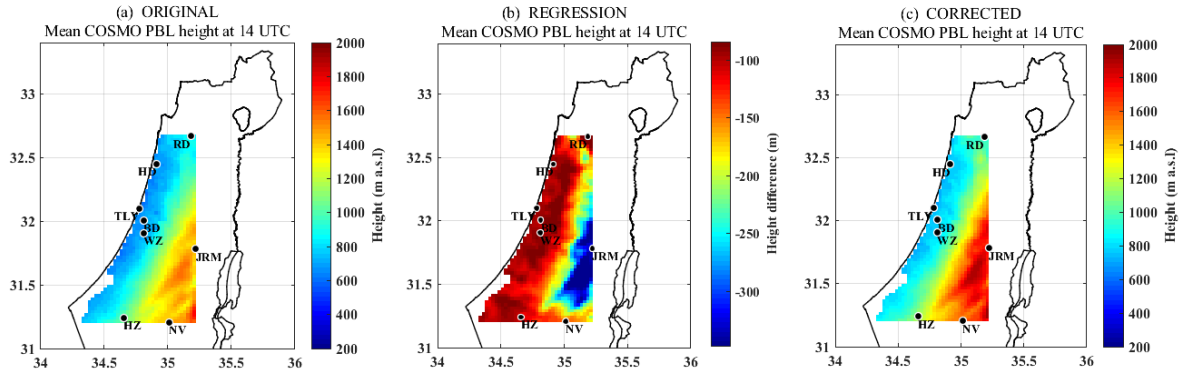


Fig. 6 3D maps of $COSMO_R$ mean PBL heights over Israel at 14 UTC before (a), and after (c) correction. The regression (b) based on Eq. (6), depicts the height difference between the results
875 from $COSMO_R$ and the ceilometers. The analysis was performed on the number of available days for each site on August 2015 as follows: Jerusalem - 21 days, Nevatim - 13 days, Hazerim - 20 days, Ramat David - 26 days, Weizmann - 25 days, Beit Dagan - 13 days, Hadera - 16 days, Tel Aviv - 25 days.